Efficient Preparation of Nanoparticles Reinforced Nickel-based Composite Coating with Highly Preferred (220) Orientation

Renjie Ji (jirenjie@163.com)
China University of Petroleum Huadong https://orcid.org/0000-0002-6329-876X

Hui Jin
China University of Petroleum Huadong

Yonghong Liu
China University of Petroleum Huadong

Tiancong Dong
China University of Petroleum Huadong

Fan Zhang
China University of Petroleum Huadong

Lilong Zhao
China University of Petroleum Huadong

Xinlei Wu
China University of Petroleum Huadong

Qiang Sun
China University of Petroleum Huadong

Peng Liu
China University of Petroleum Huadong

Hang Dong
China University of Petroleum Huadong

Chi Ma
China University of Petroleum Huadong

Dege Li
China University of Petroleum Huadong

Baoping Cai
China University of Petroleum Huadong

Original Article

Keywords: jet electrodeposition, composite coating, preferred orientation, adhesion force, corrosion resistance

Posted Date: September 18th, 2020

DOI: https://doi.org/10.21203/rs.3.rs-24701/v2

Version of Record: A version of this preprint was published on December 3rd, 2020. See the published version at https://doi.org/10.1186/s10033-020-00506-7.

ORIGINAL ARTICLE

Efficient Preparation of Nanoparticles Reinforced Nickel-based Composite Coating with Highly Preferred (220) Orientation

Renjie Ji[1†], Hui Jin[1†], Yonghong Liu[1,2*], Tiancong Dong[1], Fan Zhang[1], Lilong Zhao[1], Xinlei Wu[1], Qiang Sun[1], Peng Liu[1], Hang Dong[1], Chi Ma[1], Dege Li[1], Baoping Cai[1]

Abstract

Nanoparticles reinforced metal matrix composite coatings have great application potential in mechanical parts surface strengthening due to their excellent mechanical properties. This paper reports a phenomenon that the grain orientation gradually evolves to (220) with the deposition current density increasing when preparing nanoparticles reinforced nickel-based composite coatings by jet electrodeposition (JED). During the preparation of Ni-SiC composite coatings, the deposition current density increases from 180 A/dm^2 to 220 A/dm^2, and TC(220) gradually increases from 41.4% to 97.7% correspondingly. With the increase of TC(220), the self-corrosion potential increases from -0.575 V to -0.477 V, the corrosion current density decreases from 9.52 μA·cm^2 to 2.76 μA·cm^2, the diameter of corrosion pits that after 10 days of immersion in 3.5 wt% NaCl solution decreases from 278~944 nm to 153~260 nm, and the adhesion of the coating is increased from 24.9 N to 61.6 N. Compared with conventional electrodeposition (CED), the Ni-SiC composite coating prepared by JED has the advantages of smooth surface morphology, corrosion resistance and strong adhesion, which is more obvious with the increase of TC (220).

Keywords: jet electrodeposition, composite coating, preferred orientation, adhesion force, corrosion resistance

1 Introduction

With the continuous development of modern industry, the wear resistance and corrosion resistance of more and more key components of high-end equipment are required, so the high-performance composite coatings are usually required to be prepared on the key component surface. Nanoparticles reinforced metal matrix composite coatings have great application potential in mechanical parts surface strengthening due to their excellent hardness, abrasion resistance, corrosion resistance and high temperature oxidation resistance. It is widely concerned by researchers. Ruiqian Li et al. [1] produced the Ni-SiO_2 composite coating by electrodeposition and found that the addition of SiO_2 nanoparticles improved the wear resistance of the coating. Baosong Li et al. [2] prepared the Ni-W/TiN coating by pulse electrodeposition and observed that the doped TiN nanoparticles could promote nucleation and caused obvious changes in microstructure, thus improving the hardness and corrosion resistance of the coating. Yongqi Tao et al. [3] fabricated the Ni-B-Sc coating by conventional electrodeposition and detected that the grain boundary and phase boundary area increased due to the addition of Ni_2Sc nanoparticles. However, nanoparticles usually exist in the form of agglomeration in the plating solution because of their high surface energy. It is difficult to break the agglomeration of nanoparticles by conventional electrodeposition, so the prepared composite coatings have defects such as rough surface and poor adhesion [4, 5].

Jet electrodeposition (JED) is a kind of unconventional electrodeposition. The high-speed jet liquid improves the transmission speed of ions in the deposition process compared with conventional electrodeposition (CED). The ions are evenly distributed by high-speed flushing, which reduces the concentration polarization and improves the upper limit value of current density in the process of electrodeposition [6, 7]. Meanwhile, the agglomeration of the nanoparticles is broken up during the high-speed flushing, and the nanoparticles are distributed uniformly in the coating. Therefore, using jet electrodeposition to prepare nanoparticles reinforced composite coating, the advantages of high deposition efficiency, uniform distribution of nanoparticles and good surface quality of coating can be obtained [8-10].

During electrodeposition, the preferred orientation

*Correspondence: liuyhupc@163.com
[1] College of Mechanical and Electronic Engineering, China University of Petroleum (East China), Qingdao, Shandong, 266580, PR China 仅列出
通讯作者的第一单位，其他单位在文后统一列出
Full list of author information is available at the end of the article

(texture) often occurs, which means significant amounts of grains exhibit the same common orientation characteristics in the deposition layer. It is called highly preferred orientation if almost all of grains are assembled in one certain orientation. Through controlling the preferred orientation of the grains in the deposition layer, the properties of deposition layer can be improved, and even deposition layer has some special functions. Haibo Gao et al. [11] made Co-Ni films with preferred (220) orientation by controlling the variation of Co and Ni ratio, which showed superior photocatalytic performance. Alexandre Ponrouch et al. [12] prepared preferentially oriented (100) platinum nanowires and thin films by changing the deposition potential, which exhibited efficient electro-catalytic properties. Jiwon Kim et al. [13] manufactured $Bi_2Te_{3-x}Se_x$ thin films by pulse electrodeposition. Through changing the duty cycle of current, thin films had the preferred orientation of (110), and displayed superior thermoelectric performance.

In recent years, the research on the preferred orientation of nickel coatings by CED has attracted much attention. J.A. Calderón et al. [14] carried out the experiment about preparing Ni-SiC composite coatings. It was found that with the increase of SiC content, the grain orientation of the coatings gradually evolved from (200) to (111), and corrosion resistance of the coating was improved with the grain orientation of (111). Yuantao Zhao et al. [15] performed the research on Ni-xAl-yTi composite coatings. They claimed that as the content of Al and Ti particles increased, the orientation of (200) decreased while (111) increased, and the preferred (111) orientation coating showed better corrosion resistance than preferred (200) orientation. Morteza Alizadeh et al. [16] undertook the analysis about Ni-Cu/Al_2O_3 composite coatings. They reported the structure of coatings gradually evolved to preferred (111) orientation when the content of Al_2O_3 increased, and the hardness, wear resistance and corrosion resistance of coatings were improved. Jianhua Deng et al. [17] demonstrated that with the addition of 1,4-bis(2-hydroxyethoxy)-2-butyne (BEO), the grains preferred orientation of Ni/diamond composite coatings changed to (200), and the wear resistance of the coating was also enhanced.

The above studies on the preferred orientation of nickel-based composite coatings mainly focused on (111) and (200), and little research about the highly preferred (220) orientation. This paper reveals the principle of efficient preparation nanoparticles reinforced nickel-based composite coating with highly preferred (220) orientation, and then explores the effect of deposition parameters on the structure of nanoparticles reinforced nickel-based composite coatings. Because of the high hardness and stability of SiC nanoparticles, Ni-SiC composite coatings have been widely used [18]. This paper focused on the properties of Ni-SiC composite coatings. The microstructure, corrosion resistance and the adhesion force of the Ni-SiC composite coating with highly preferred (220) orientation were investigated. Some innovative theoretical and technological achievements have been made.

2 Experimental

2.1 Principle of efficient preparation of nanoparticles reinforced nickel-based composite coating by JED.

The experimental device for JED is shown in Figure 1a. The pure titanium rod connects to the positive pole of DC power supply and the substrate connects to the negative pole of DC power supply. The pure titanium rod acts as the current transfer electrode, which transfers the current to nickel balls, making nickel balls become anode. Nickel atoms are oxidized into a large amount of Ni^{2+}, which are used to supplement the Ni^{2+} constantly consumed in the plating solution. The titanium rod is not consumed in experiments because the chemical properties of titanium rod is more stable than those of nickel balls. Due to the titanium rod is closer to the upper surface of the substrate, the unconsumed titanium rod can play a role in providing a stable electric field environment, and the deposited coatings have better uniformity. The plating solution in the liquid storage tank is heated by a water bath to maintain a constant temperature. During the preparation process, firstly the composite plating solution is transported to the anode cylinder through the inlet pipe by a diaphragm pump. Then the plating solution in the anode cylinder is impacted on the substrate through the nozzle at a high speed for deposition. Finally, the plating solution flows back to the liquid storage tank through the outlet pipe.

The schematic diagram of preparation principle of nanoparticles reinforced nickel-based composite coatings by JED is illustrated in Figure 1b. Most of the nanoparticles exist in the plating solution as agglomeration, which mainly are surrounded by water molecules and ion clusters. Since mainly chemical reaction is the redox of Ni^{2+} during electrodeposition, so the model is simplified into nanoparticles agglomeration surrounded by a large number of Ni^{2+}. When the nanoparticles agglomeration is impacted the substrate at a high speed, the nanoparticles agglomeration are divided into many individual nanoparticles due to reacting force. According to the composite co-deposition theory [19, 20], some

nanoparticles are adsorbed on the substrate, among which the strongly adsorbed nanoparticles are deposited and the weakly adsorbed nanoparticles are washed away. Meanwhile, under the condition of high deposition current density, a large amount of Ni^{2+} near the cathode are reduced to Ni atoms, and then Ni atoms are deposited on the substrate. The stacking of Ni atoms and nanoparticles covering substrate defects rapidly, and eventually the nanoparticles reinforced nickel-based composite coating with smooth surface is formed.

As shown in Figure 1c, the thickness of the coating increase gradually when the nozzle moves back and forth along the path at a certain scanning speed. The required thickness and shape of the composite coating has been obtained by controlling the nozzle path and deposition time.

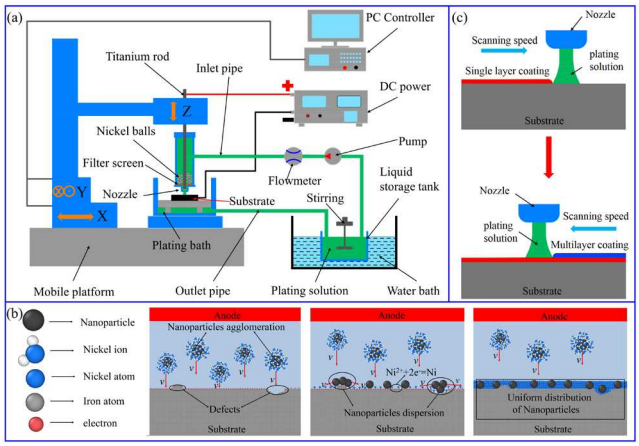

Figure 1 Schematic diagram of **(a)** experimental device for JED, **(b)** preparation principle of nanoparticles reinforced nickel-based composite coatings, **(c)** production process of nanoparticles reinforced nickel-based composite coatings.

2.2 Experimental parameters of preparation of nanoparticles reinforced nickel-based composite coating by JED.

The composition of plating solution and experimental parameters are shown in Table 1.The purity of SiC nanoparticles is 99.99% and the average particle size is about 50 nm (Figure 2a-2b). and the SEM figures are shown in figure 2a-b. The substrate material is medium carbon steel. Before the experiment, the substrate is pretreated. The process is as follows: fine grinding - oil removal - acetone ultrasonic cleaning - alcohol ultrasonic cleaning - deionized water ultrasonic cleaning - drying. The XRD pattern of the substrate is shown in Figure 2c.

Table 1 The composition of plating solution and experimental parameters.

Composition and parameters	Quantity
$iSO_4 \cdot 6H_2O$ (g/L)	300
$NiCl_2 \cdot 6H_2O$ (g/L)	40
H_3BO_4 (g/L)	40
Saccharin (g/L)	0.5
Emulsifier OP-10 (g/L)	1.0
SiC nano-particles (g/L)	3.0
pH value	4.0
Nozzle diameter (mm)	5.0
Scanning speed of nozzle (mm/min)	100
Distance between nozzle and cathode (mm)	3.0
Injection velocity (m/s)	1.40~2.65
Current density (A/dm^2)	180~220
Temperature (℃)	60

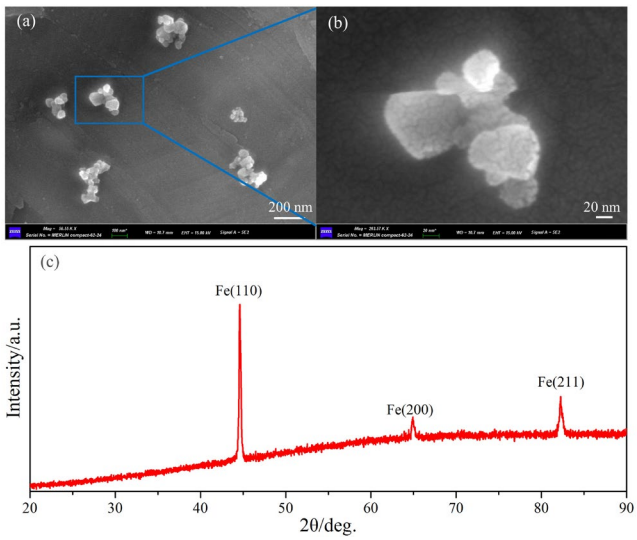

Figure 2 The morphology and composition of SiC nanoparticles: **(a)** SEM image, **(b)** enlarged image, **(c)** XRD pattern of substrate.

2.3 Testing details.

The grain orientation and grain size of nanoparticles reinforced nickel-based composite coatings are characterized by X-ray diffraction (XRD, X'Pert Pro MPD) with Cu-Kα (λ=0.154184 nm) radiation, and the test parameters are voltage of 45 kV, current of 40 mA, scanning range of 20°~90°, step width of 0.01° and scanning speed of 10°/min. The adhesion force of nanoparticles reinforced nickel-based composite coatings are quantitatively texted by scratch tester (WS-2004). The test is carried out in the form of dynamic loading. The scratch length is 4 mm, and the diamond tool is uniformly loaded from 0~70 N at a loading rate of 70/4 N·mm-1. The morphology and element content of nanoparticles reinforced nickel-based composite coatings are measured by scanning electron microscope with energy dispersive spectroscopy (SEM, EDS, ZEISS MERLIN Compact). The surface roughness of nanoparticles

reinforced nickel-based composite coatings are measured by TR300 Roughness Measuring Instrument and the sampling length is 4 mm. The electrochemical properties of Ni-SiC composite coatings are performed by electrochemical workstation (CHI 760e) in 3.5 wt% NaCl solution at the room temperature. The test samples are Ni-SiC composite coatings with an area of 1 cm^2. A saturated calomel electrode, platinum plate and samples are used as the reference electrode, counter electrode and working electrode, respectively. The polarization curves are recorded through the potential range of -150 mV to +350 mV (compared to the Eocp) at a scan rate of 0.002 V/s and a scan frequency of 2 Hz. The electrochemical impedance spectroscopy (EIS) investigations are generated in the sinusoidal signal amplitude of 10 mV and at a frequency range of 10^5 ~10^{-2} Hz. The full immersion corrosion tests of Ni-SiC composite coatings are carried out. The corrosion solution was 3.5 wt% NaCl solution, and the corrosion time is 1 day, 3 days, 5 days and 10 days, respectively.

3 Results and discussion

3.1 The grain orientation evolution of Ni-SiC composite coating during JED.

In the process of JED, the deposition layer is rapidly formed on the surface of the substrate with the condition of high current density by means of high-speed jetting. Therefore, the parameters of injection velocity and current density are important factors influencing the structure of the coatings. In this paper, a large number of Ni-SiC composite coatings are produced at different current densities and different injection velocities. The thicknesses of these coatings are all controlled to be about 50 μm by changing the deposition time. According to Figure 3a-3e, the XRD patterns of Ni-SiC composite coatings prepared by JED under different deposition parameters all present clear diffraction peaks of Ni(111), Ni(200), and Ni(220). It can be seen that with the increase of the deposition current density from 180 A/dm^2 to 220 A/dm^2, the coating orientation shows a trend of gradual evolution to Ni(220). The XRD pattern of the Ni-SiC composite coating prepared by CED is shown in Figure 3f, which indicates that the Ni-SiC composite coating without highly preferred (220) orientation.

The preferred orientation coefficient (texture coefficients) of different crystal planes in coating of these coatings are calculated by formula (1) [21], where TC(hkl) is the texture coefficient of (hkl) orientation, I(hkl) is measured intensity of (hkl) reflection, I0(hkl) is powder diffraction intensity of nickel (PDF#70-0989), and n is the number of reflections used in the calculations. In this case, (111), (200) and (220) peaks were used for texture coefficient calculation (n = 3).

$$\mathrm{TC}(hkl) = \frac{I_{(hkl)} / I_{0(hkl)}}{\sum_{i=1}^{n} I_{(hkl)} / I_{0(hkl)}}, \quad (1)$$

The grain sizes of these coatings are calculated by formula (2) [22], where D(hkl) represents grain size of (hkl) orientation, B represents half-height width of diffraction peak (degree), γ represents the wavelength of Cu-Kα (λ=0.154184 nm), θ represents Bragg angle (rad) and K represents the constant (K = 0.89).

$$\mathrm{D}(hkl) = \frac{K\gamma}{B\cos\theta}, \quad (2)$$

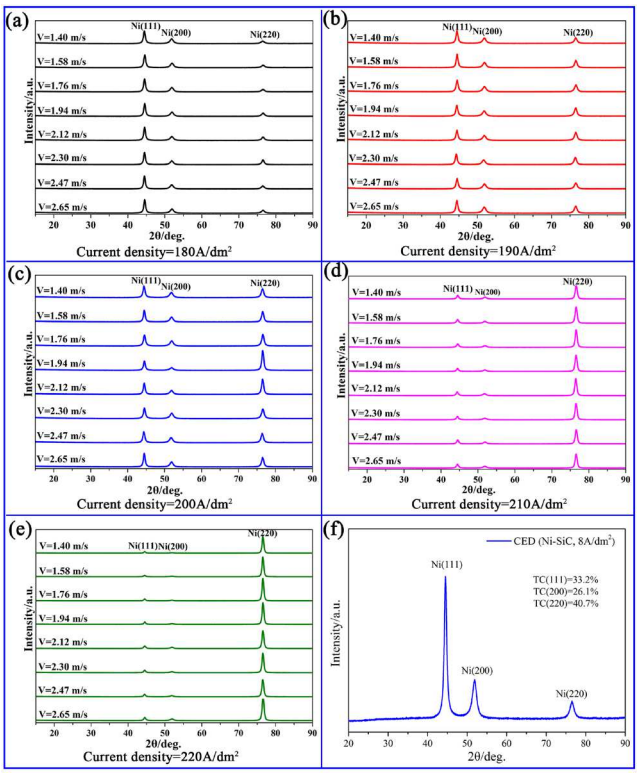

Figure 3 **(a-e)** XRD patterns of Ni-SiC composite coatings prepared by JED under different deposition parameters, **(f)** XRD pattern of Ni-SiC composite coating prepared by CED.

Figure 4a-4c demonstrates the variation of TC(111), TC(200) and TC(220) of Ni-SiC composite coatings prepared by JED under different deposition parameters. With the current density increases, it shows a general trend that TC(111) and TC(200) gradually decreases and TC(220) gradually increases. At low current density conditions (180 A/dm^2-200 A/dm^2), the TC(111), TC(200) and TC(220) are greatly affected by variation of injection velocity. As the

injection velocity increases, TC(111) and TC(200) decreases first and then increases, and TC(220) increases first and then decreases. However, at a higher deposition current density (> 200 A/dm^2), the grain orientation of the coatings are little affected by variation of injection velocity, and the TC(111), TC(200) and TC(220) remains stable value. Under the deposition conditions of 220 A/dm^2 current density and 1.76 m/s injection velocity, TC(220) reaches a maximum of 97.7%.

As shown in Figure 4d, it can be seen that the variation range of D(111) and D(200) is small with the current density increased. D(111) is between 19~20 nm and D(200) is between 17~18 nm. Unlike D(111) and D(200), D(220) increases with the increase of deposition current density. When the deposition current density is 180 A/dm^2, the average value of D(220) is 47.5 nm. As the deposition current density increases to 220 A/dm^2, the average value of D(220) increases to 61.6 nm.

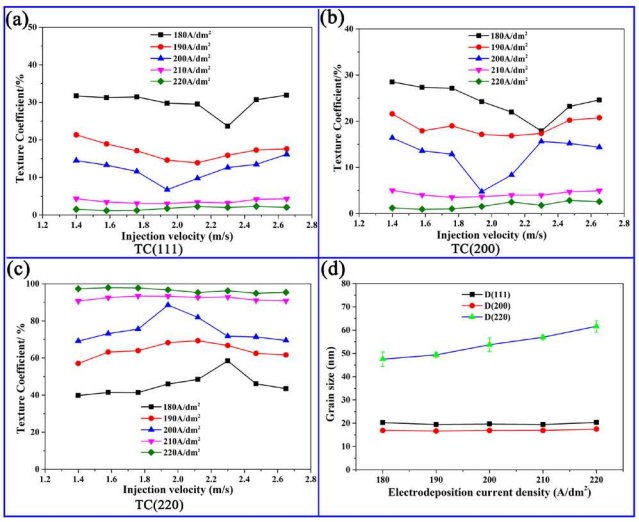

Figure 4 **(a-c)** The texture coefficients of Ni-SiC composite coatings prepared by JED under different deposition parameters: **(a)** TC(111), **(b)** TC(200), **(c)** TC(220). **(d)** The grain size statistic of Ni-SiC composite coatings prepared by JED under different deposition parameters.

As shown in Figure 5, in the process of preparing nanoparticles reinforced nickel-based composite coatings by JED, Ni atoms are stacked with face centered cubic structure cells. Usually, those cells are deposited on the substrate surface with (111) crystalline plane, (200) crystalline plane, and (220) crystalline plane. The selection of grains orientation mainly depends on cathodic overpotential, which is mainly determined by the deposition current density according to the Tafel formula. Under the condition of low deposition current density, the grain orientation of coating tended to (111). With the deposition current density increasing, the grain orientation of coating gradually evolves to (220). When the deposition current density exceeds a certain value, most of the cells are adsorbed on the substrate with the (220) crystalline plane.

Compared with the influence of deposition current density, the effect of injection velocity on the grain orientation of the coating is smaller. Because the bonding strength of (111) and (200) oriented grains to the substrate is less than that of (220) oriented grains, the increase of injection velocity makes the nickel structure cells tend to adsorb on the substrate with (220) crystalline plane. However, the TC(220) of the coating does not increase monotonically with the increase of the injection velocity. There is a critical value for the injection speed. When the injection speed exceeds this value, the nickel structure cells tend to adsorb on the substrate with random crystalline planes instead. The critical value has a negative correlation with the deposition current density, that is, the smaller the deposition current density, the larger the critical value.

Under the condition of high deposition current density, the nickel structure cells nucleate rapidly, and the number of crystal nucleus with (220) orientation is larger than that of with (111) orientation and (200) orientation. Therefore, the crystal nucleus with (220) orientation dominate the growth process. Eventually, the average size of (220) orientation grains is obviously larger than that of (111) orientation grains and (200) orientation grains.

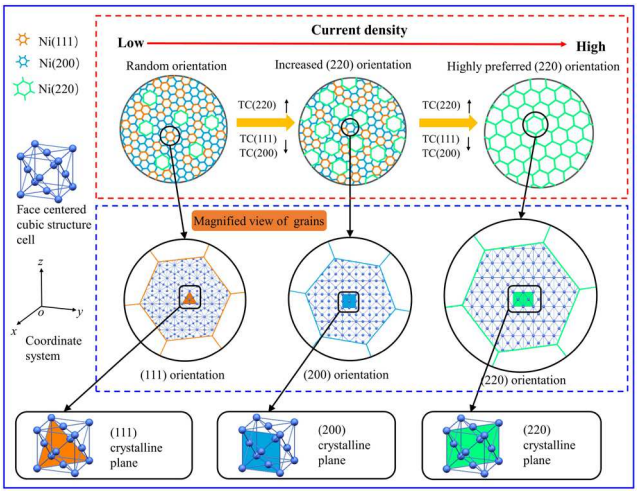

Figure 5 Schematic diagram of the evolution of grain orientation in the process of preparing nanoparticles reinforced nickel-based composite coatings by JED.

3.2 The morphology of Ni-SiC composite coating with highly preferred (220) orientation.

Figure 6 shows the morphology of a Ni-SiC composite

coating with highly preferred (220) orientation prepared by JED (TC(220) = 97.7%). As shown in Figure 6a, the surface (Area C) and section (Area f) of the coating are observed. It is obvious that the surface of Ni SiC composite coating with highly preferred (220) orientation is compact and flat (Figure 6c, Figure 6f), and there is no dome-like or hill valley like structure [16, 23-25]. The surface roughness of the coating is Ra0.119 μm (Figure 6b). SiC nanoparticles have no agglomeration inside the coating (Figure 6d, Figure 6g) and are evenly distributed in different areas of the coating (Figure 6e, Figure 6h).

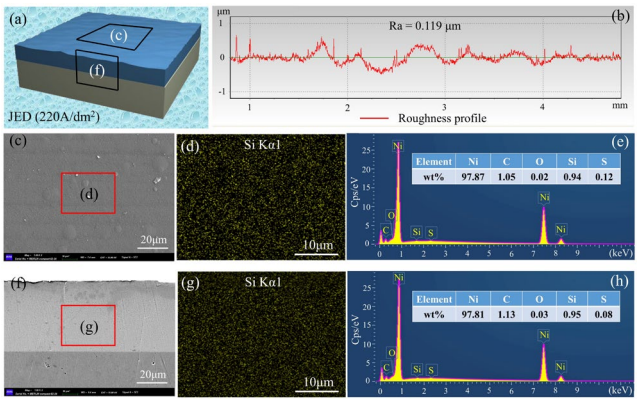

Figure 6 The morphology of the Ni-SiC composite coating with highly preferred (220) orientation prepared by JED: **(a)** schematic diagram of detection area, **(b)** roughness profile of the coating surface, **(c)** microstructure of the coating surface, **(d)** distribution of SiC nanoparticles on the coating surface, **(e)** EDS map of the coating surface, **(f)** microstructure of the coating section, **(g)** distribution of SiC nanoparticles on the coating section, **(h)** EDS map of the coating section.

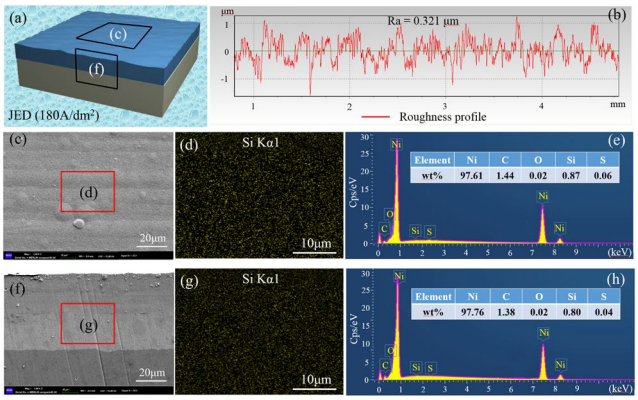

Figure 7 The morphology of the Ni-SiC composite coating without highly preferred (220) orientation prepared by JED: **(a)** schematic diagram of detection area, **(b)** roughness profile of the coating surface, **(c)** microstructure of the coating surface, **(d)** distribution of SiC nanoparticles on the coating surface, **(e)** EDS map of the coating surface, **(f)** microstructure of the coating section, **(g)** distribution of SiC nanoparticles on the coating section, **(h)** EDS map of the coating section.

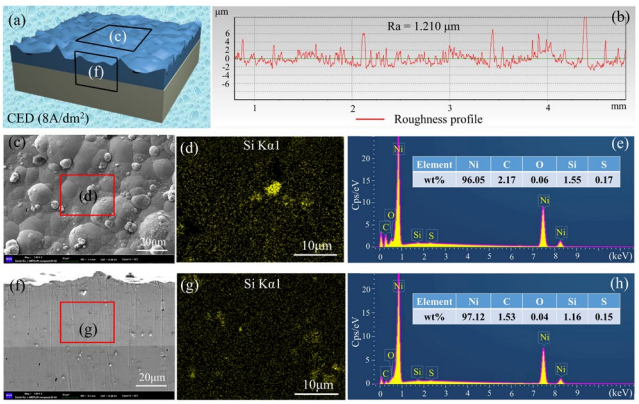

Figure 8 The morphology of the Ni-SiC composite prepared by CED: **(a)** schematic diagram of detection area, **(b)** roughness profile of the coating surface, **(c)** microstructure of the coating surface, **(d)** distribution of SiC nanoparticles on the coating surface, **(e)** EDS map of the coating surface, **(f)** microstructure of the coating section, **(g)** distribution of SiC nanoparticles on the coating section, **(h)** EDS map of the coating section.

Figure 7 shows the morphology of a Ni-SiC composite coating without highly preferred (220) orientation prepared by JED (TC(220) = 41.4%). As shown in Figure 7a, the surface (Area C) and section (Area f) of the coating are observed. It is obvious that the surface of Ni SiC composite coating has slight bumps and gullies. The surface roughness of the coating is Ra0.321 μm (Figure 7b). SiC nanoparticles have no agglomeration inside the coating (Figure 7d, Figure 7g) and are evenly distributed in different areas of the coating (Figure 7e, Figure 7h).

Figure 8 shows the morphology of a Ni-SiC composite coating prepared by CED (TC(220) = 40.7%). As shown in Figure 8a, the surface (Area C) and section (Area f) of the coating are also observed. The surface of Ni SiC composite coating prepared by CED is coarse and fluctuant (Figure 8c, Figure 8f). The surface roughness of the coating is Ra1.210 μm (Figure 8b). SiC nanoparticles have obvious agglomeration inside the coating (Figure 8d, Figure 8g) and the content varies greatly at different areas (Figure 8e, Figure 8h).

Compared with the coating prepared by CED, The high speed jetting process in JED can make SiC nanoparticles evenly distributed in the coating and the surface quality of the coating prepared by JED is obviously improved due to the high speed scouring of the plating solution. For JED, the the Ni-SiC composite coating with highly preferred (220) orientation has smoother surface topography, which is beneficial to significantly improve the corrosion resistance

of Ni-SiC composite coating.

3.3 The corrosion resistance of Ni-SiC composite coating with highly preferred (220) orientation.

In this paper, the corrosion resistance of Ni-SiC composite coating is tested, including electrochemical test and full immersion corrosion test. Figure 9 reports the electrochemical test results of Ni-SiC composite coatings in 3.5 wt% NaCl solution. The dynamic polarization curves are shown in Figure 9a. As can be seen from this figure, the corrosion potential (E_{corr}) and corrosion current density (i_{corr}) of the Ni-SiC composite coating prepared by CED are -0.747 V and 54.52 μA·cm^2, respectively.

The Ni-SiC composite coatings are prepared by JED at an injection velocity of 1.76 m/s and a current density of 180~220 A/dm^2. With the increase of the deposition current density, the TC(220) of the coating increases from 41.4% to 97.7%, the corrosion potential of the coating increases from -0.575 V to -0.477 V, and the corrosion current density decreases from 9.52 μA·cm^2 to 2.76 μA·cm^2. This indicates that the corrosion resistance of the coating is enhanced. EIS is a powerful and non-destructive electrochemical technology to confirm electrochemical reaction and study the corrosion behavior of electrode/electrolyte interface [26-29]. Figure 9b shows the typical Nyquist plots of the Ni-SiC composite coatings. A depressive semicircle can be found on each curve, indicating that the electrochemical mechanism is controlled by the charge-transfer process [30]. It can be seen that the diameter of capacitive loop increases with the increases of TC(220) of Ni-SiC composite coating. The larger the diameter of the capacitive loop, the stronger the corrosion resistance of the coating. Figure 9c shows the Bode plots of log(f) vs. log(|Z|) of the Ni-SiC composite coatings. In the high-frequency region (10^4~10^5 Hz), the values of log|Z| are similar, indicating that these are impedance values of 3.5 wt% NaCl solution. In the low-frequency region (10^{-2}~10^{-1} Hz), the impedance values of different Ni-SiC composite coatings are significantly different. For instance, at the fixed 0.01 Hz, the log(|Z|) of Ni-SiC composite coating prepared by CED is 3.41, and the log(|Z|) of Ni-SiC composite coating prepared by JED increase from 3.99 to 4.72 as the TC(220) increase from 41.4% to 97.7%. The higher the impedance value, the stronger the corrosion resistance of the coating. Figure 9d shows the Bode plots of log(f) vs. Angle of the Ni-SiC composite coatings. For the Ni-SiC composite coatings, the higher phase angle at middle high frequency for the chemical conversion treated specimen corresponds to a capacitive behavior, that is to say the conversion coating has good dielectric property to avoid the ionic flow of electrolyte [30]. When the frequency is in the range of 10^0~10^5 Hz, the phase angle of Ni-SiC composite coating prepared by CED is minimum, and the phase angle of Ni-SiC composite coating prepared by JED increases with the increase of TC(220).

The EIS data is fitted by calculated by electrical equivalent circuit (EEC). The corrosion process of Ni-SiC composite coating can be replaced by EEC of R(Q(R(QR))) when the oxide layer on the substrate surface is taken into account [31].

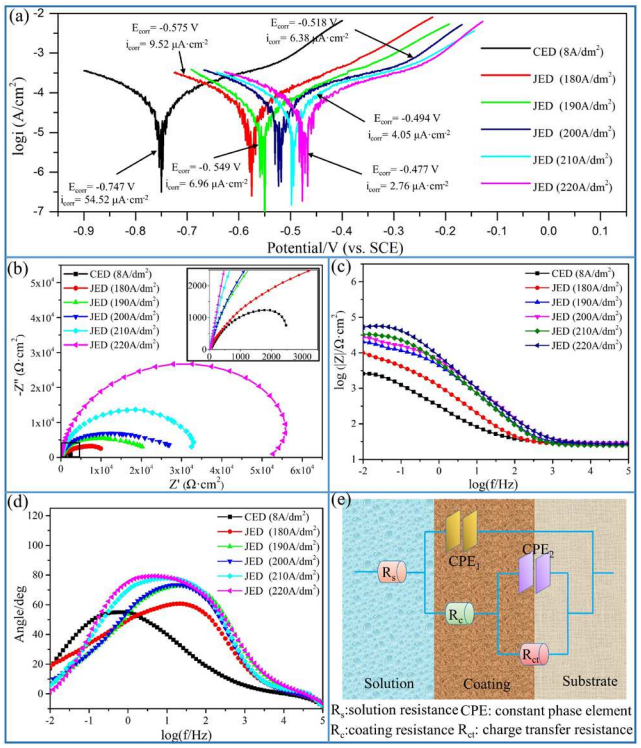

Figure 9 Electrochemical test results of Ni-SiC composite coatings: (a) dynamic polarization curves, (b) Nyquist plots, (c) Bode plots of log(f) vs. log(|Z|), (d) Bode plots of log(f) vs. Angle, (e) schematic diagram of the EEC.

As observed in Figure 9e, The EEC is consisted of the R_s modeling the solution resistance, in sequence with a constant phase element CPE_1 in parallel with another resistance R_c modeling the coating resistance, and then another constant phase element CPE_2 and the third charge transfer resistance of R_{ct} associating with the corrosion process. The impedance of CPE is defined formula (3)

$$Q_{CPE} = [Y_0(jw)^n]^{-1}, \quad (3)$$

where w is the angular frequency (rad s^{-1}), Y0 is the CPE admittance, j is the imaginary number ($\sqrt{-1}$), and n with a value of 0-1 represents the relaxation dispersion. When the

value of n is 1, the CPE is a pure capacitor with a capacitance of Y_0. It is believed that the smaller the n value is and the more defects will be on the surface as well as the pitting corrosion is more likely to occur [30, 32].

The fitting results is shown in Table 2. It can be seen that the R_c and R_{ct} of Ni-SiC composite coating prepared by CED is 1.476×10^2 Ω·cm^2 and 3.846×10^3 Ω·cm^2, respectively. Compared with that of other coatings, these parameters is the minimum value, which means this coating has the worst corrosion resistance. The Ni-SiC composite coatings prepared by JED increase with TC (220) from 41.4% to 97.7%, the R_c of the coatings increase from 4.423×10^3 Ω·cm^2 to 7.025×10^3 Ω·cm^2, and the Rct increase from 1.267×10^4 Ω·cm^2 to 5.989×10^4 Ω·cm^2 It is proved that the corrosion resistance of Ni-SiC composite coating increases with the increase of TC(220).

Table 2 Parameters fitted from EEC.

Preparation method	TC(220) /%	R_s /Ω·cm^2	CPE_1		R_c /Ω·cm^2	CPE_2		R_{ct} /Ω·cm^2
			Y_1(S·cm^{-2}·s^n)	n_1		Y_2(S·cm^{-2}·s^n)	n1	
CED (8A/dm^{-2})	40.7	28.37	8.579×10^{-4}	0.6753	1.476×10^2	8.759×10^{-4}	0.6846	3.846×10^3
JED (180A/dm^{-2})	41.4	25.83	1.661×10^{-4}	0.5643	4.423×10^3	1.658×10^{-4}	0.5635	1.267×10^4
JED (190A/dm^{-2})	63.9	28.32	3.686×10^{-5}	0.8795	1.159×10^3	4.880×10^{-5}	0.5677	2.119×10^4
JED (200A/dm^{-2})	75.6	28.83	2.588×10^{-5}	0.8722	1.571×10^3	3.386×10^{-4}	0.6184	2.608×10^4
JED (210A/dm^{-2})	93.4	24.97	3.543×10^{-5}	0.8938	2.309×10^3	2.463×10^{-5}	0.7570	3.499×10^4
JED (220A/dm^{-2})	97.7	28.04	6.916×10^{-6}	0.8984	7.025×10^3	1.566×10^{-5}	0.8623	5.989×10^4

The central area of the coatings after immersion corrosion are observed, and the surface morphologies of different corrosion times are shown in Figure 10 ~ Figure 13.

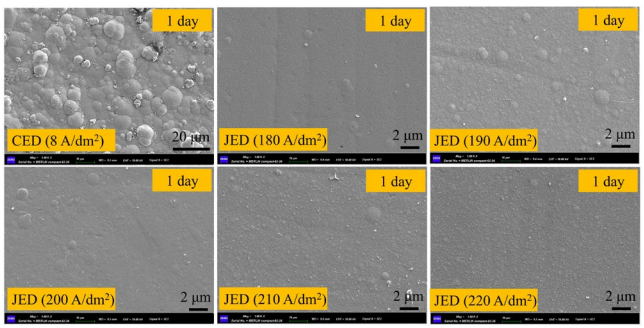

Figure 10 The surface morphologies of different Ni-SiC composite coatings after 1 day of immersion corrosion in 3.5 wt% NaCl solution

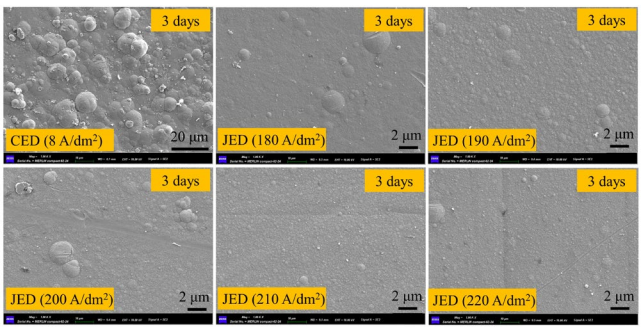

Figure 11 The surface morphologies of different Ni-SiC composite coatings after 3 days of immersion corrosion in 3.5 wt% NaCl solution.

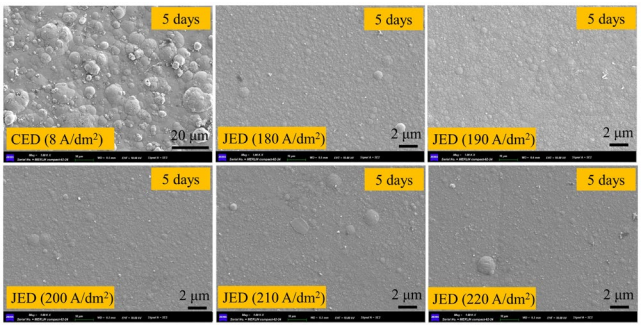

Figure 12 The surface morphologies of different Ni-SiC composite coatings after 5 days of immersion corrosion in 3.5 wt% NaCl solution.

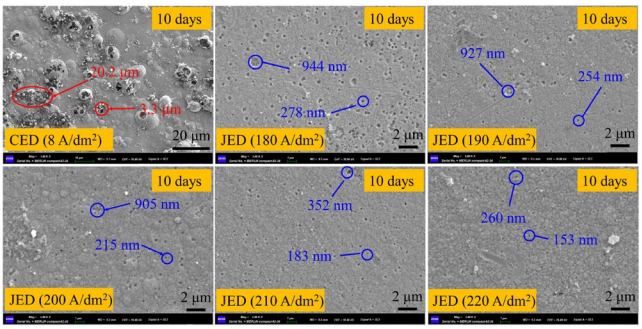

Figure 13 The surface morphologies of different Ni-SiC composite coatings after 10 days of immersion corrosion in 3.5 wt% NaCl solution.

It is obvious that when the corrosion time is 1,3 and 5 days,

the central area of different coatings is almost unchanged, indicating that the corrosion has not extended to the central area. When the corrosion time is 10 days, corrosion pits of different sizes appeared on the central surface of those coatings. Figure 13a is the surface morphology of Ni-SiC composite coating prepared by CED after 10 days of immersion corrosion. It can be found that many corrosion products adhere to the surface of the coating, and the size of corrosion pits is about 3.3~22.2 μm. Figure 13b-13f are the surface morphologies of Ni-SiC composite coatings prepared by JED after 10 days of immersion corrosion. Compared with Figure 13a, there are no obvious corrosion products on the surface of the coating, and the corrosion pits are all less than 1 μm. When the TC(220) of the coating is 41.4%, the size of corrosion pits is about 278~944 nm (Figure 13b). When the TC(220) of the coating is 63.9%, the size of corrosion pits is about 254~927 nm (Figure 13c). When the TC(220) of the coating is 75.6%, the size of corrosion pits is about 215~905 nm (Figure 13d). When the TC(220) of the coating is 93.4%, the size of corrosion pits is about 183~352 nm (Figure 13e). When the TC(220) of the coating is 97.7%, the size of corrosion pits is about 153~260 nm (Figure 13f). This shows that as the TC(220) increases, the corrosion resistance of the Ni-SiC composite coating is improved.

Surface quality is the most important factor affecting the corrosion resistance of the coating. The corrosion resistance of the coating decreases with the increase of the number of surface defects. There are many defects on the surface of Ni-SiC composite coating prepared by CED, such as the agglomeration of SiC nanoparticles, pinholes and pockmarks. Corrosion occurs preferentially at these defect locations, and over a period of time, it is easy to cause SiC agglomerated particles to fall off, resulting in the formation of holes in the coating, which eventually form larger corrosion pits with the increase of corrosion time. The surface of Ni-SiC composite coatings prepared by JED are compact and flat without obvious defects and SiC particles agglomeration, so the corrosion resistance of coatings are significantly improved. The corrosion pits occur uniformly at the grain boundaries on the coating surface, and the corrosion pits gradually expanded with the increase of corrosion time. Under the same corrosion area, the smaller the grain boundaries proportion and the less the number of corrosion pits. With the increase of deposition current density, the grain size of Ni-SiC composite coating also increases, and the proportion of grain boundaries decreases. At the same time, with the increase of TC(220), the coating with the same orientation gradually formed. The dislocations and other defects at grain boundaries are also reduced and the diffusion rate of corrosion pits is reduced. Therefore, the Ni-SiC coating with highly preferred (220) orientation shows excellent corrosion resistance.

3.4 The adhesion force of Ni-SiC composite coating with highly preferred (220) orientation.

The adhesion force is an important index to judge the performance of coating. The higher the adhesion force of the coating, the less easy it will fall off, and the longer the service life will be. In this paper, the adhesion of Ni-SiC composite coatings and substrate is quantitatively measured by scratch method. Figure 14a shows the scratch morphology of Ni-SiC composite coating prepared by CED, and Figure 14b-14f show the scratch morphologies of Ni-SiC composite coatings prepared by JED under the deposition current density of 180~220 A/dm^2. As shown in the elliptical frame selection area, the load corresponding to the first crack position of the coating is defined as the value of adhesion force, which is 20.5 N、24.9 N、46.8 N、55.2 N、60.5 N and 61.6N, respectively. It can be seen that the adhesion force of Ni-SiC composite coating has a positive correlation with the value of TC(220). The higher TC (220), the higher the adhesion force of the coating.

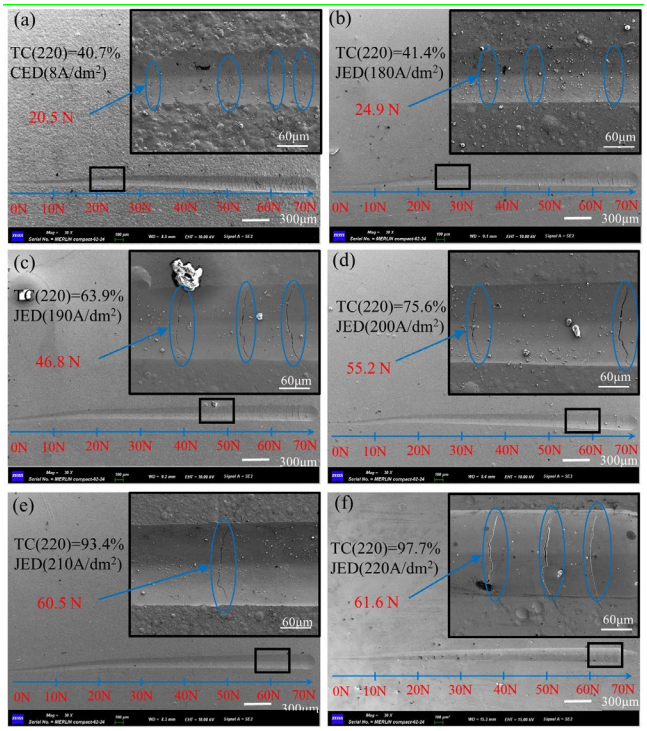

Figure 14 (a-f) Scratch morphology of different Ni-SiC composite coatings: (a) CED (8 A/dm2), (b) JED (180 A/dm2), (c) JED (190 A/dm2), (d) JED (200 A/dm2), (e) JED (210 A/dm2), (f) JED (220 A/dm2).

From the microscopic point of view, the adhesion force between coating and substrate depends on the contact strength of interface. A fundamental quantity determining the strength of interface is the ideal work of adhesion (Wad), which is the work spent on separation the interface into two free surface. The work of adhesion between coating and substrate can be calculated by the Formula (4) [33, 34].

$$W_{ad} = (E_{slab1} + E_{slab2} - E_{int}) / A, \quad (4)$$

Where E_{slab1} and E_{slab1} are the total energies of slab1 and slab2, E_{int} is the total energy of the interface system including slab1 and slab2, and A is the interface area.

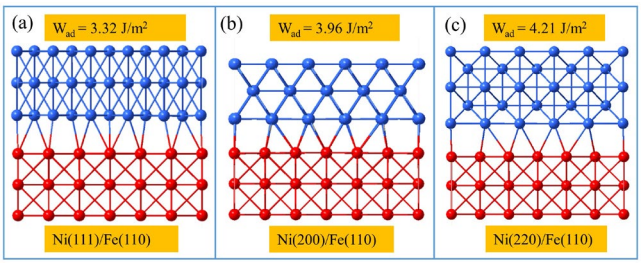

Figure 15 DFT optimized structures of **(a)** Ni(111)/Fe(110), **(b)** Ni(200)/Fe(110) and **(c)** Ni(220)/Fe(110) interfaces.

The DFT simulation models are shown in Figure 15.The substrate is medium carbon steel, the main orientation of the substrate is Fe(110). The W_{ad} of Ni(111)/Fe(110), Ni(200)/Fe(110), and Ni(220)/Fe(110) interfaces are 3.32 J/m^2, 3.96 J/m^2 and 4.21 J/m^2, respectively. The W_{ad} of Ni(220)/Fe(110) interface is more than that of Ni(111)/Fe(110) interface and Ni(200)/Fe(110) interface, indicating that the adhesion force between Ni-SiC composite coating with highly preferred (220) orientation and substrate is higher.

4 Conclusions

(1) The grain orientation of Ni-SiC composite coatings prepared by JED gradually evolves to (220) with the increase of current density. The Ni-SiC composite coating with highly preferred (220) orientation is prepared at current density of 220 A/dm^2, while the orientation coefficient reached to 97.7%.

(2) In the process of JED, the high-speed jetting fluid makes the nanoparticles break the agglomeration state and disperse evenly into the coating. Under the condition of high current density, the deposition layer quickly to fill the defects of the substrate and form a compact and flat composite coating on the surface. The surface roughness of Ni-SiC composite coating with highly preferred (220) orientation is 90.2% lower than that of Ni-SiC composite coating prepared by CED.

(3) The corrosion resistance of Ni-SiC composite coatings increases with the increase of TC(220). Compared with the corrosion resistance of coating prepared by CED, the corrosion resistance of coating with highly preferred (220) orientation prepared by JED has a 36.1% increase in corrosion potential and a 94.9% decrease in corrosion current density.

(4) DFT simulation is used to calculate the ideal work of adhesion of Ni(111)/Fe (110) interface, Ni(200)/Fe(110) interface, and Ni(220)/Fe(110) interface of the Ni-SiC composite coating, among which Ni(220)/Fe(110) interface has higher Wad than Ni(111)/Fe (110) interface and Ni(200)/Fe(110) interface. The Ni-SiC composite coating with a highly preferred (220) orientation obtains the maximum adhesion force, and the adhesion force is 200% higher than that of the Ni-SiC composite coating prepared by CED.

Authors' Contributions

Renjie Ji and Hui Jin contributed equally. The manuscript was written by Renjie Ji, Yonghong Liu and Hui Jin. Experiments were designed by Tiancong Dong, Fan Zhang, Lilong Zhao and Chi Ma. Xinlei Wu, Qiang Sun, Hang Dong, Dege Li, Peng Liu and Baoping Cai performed the experiments. All authors have given approval to the final version of the manuscript.

Author Details

[1]College of Mechanical and Electronic Engineering, China University of Petroleum (East China), Qingdao, Shandong, 266580, PR China. [2] Key Laboratory of Unconventional Oil & Gas Development, China University of Petroleum (East China), Ministry of Education, Qingdao PR China. †These authors contributed equally to this work and should be considered as the co-first authors.

Authors' Information

Renjie Ji received his Ph.D. degree in Mechanical and Electronic Engineering from *China University of Petroleum* in 2011. Now he is the professor of *China University of Petroleum*, the "Hong Kong Scholar" visiting researcher of *Hong Kong Polytechnic University*. He is the council member of *Chinese Nontraditional Machining Society*, the vice director of *Youth Committee of Chinese Nontraditional Machining Society* and the member of National Technical Committees 161 on Nontraditional Machine Tools of Standardization Administration of China. His research

interest focuses on technology and theory of nontraditional machining. E-mail: jirenjie@163.com.

Hui Jin, born in 1994, received bachelor's degree of mechanical engineering from *China University of Petroleum (East China)* in 2016, and now working towards his PhD at *China University of Petroleum (East China)*. His research interests involve the Jet electrodeposition technology and material surface strengthening technology. Tel: +86-15621465936; E-mail: jinhui_upc@163.com.

Yonghong Liu received his Ph.D. degree in Mechanical Design, Manufacturing and Automation from *Harbin Institute of Technology* in 1996. He is currently a professor in *China University of Petroleum*, where he is also the Dean of the College of Mechanical and Electronic Engineering. He enjoys the special government allowances issued by the State Council. His research interests include development of subsea engineering equipment, manufacturing technology of offshore equipment and fault diagnosis methodology. E-mail: liuyhupc163.com.

Tiancong Dong, born in 1997, is currently a Master Degree Candidate at Mechanism laboratory of Mechanical Engineering, *China University Of Petroleum, China*. He received his bachelor degree from *China University of petroleum, China*, in 2019. His research interests include Jet electrodeposition and Electrochemical behavior of coatings. Tel: +86-17806247069; E-mail: 1219498227@qq.com.

Fan Zhang，born in 1991, is currently a Ph.D. candidate in Prof. Renjie Ji group at *College of Mechanical and Electronic Engineering in China University of Petroleum (East China)*. His research interest focuses on the electrochemical energy conversion and storage using transitional metal-based catalyst. Tel: +86-15192535830; E-mail:1055959043@qq.com.

Lilong Zhao awarded master degree of Mechanical Engineering (smart product design) from *Nanyang Technological University Singapore* in 2016. He used to be a mechanical design engineer in MCE Singapore and mechatronics engineer in *ALPS-Tech China*. Currently, he is a Ph.D. candidate major in mechanical engineering in *China University of Petroleum*. Mainly research fields are intelligent manufacturing, electrical discharge machining, robot technology and ergonomics. Tel: +86-19954262295; E-mail: lilong.zhao@outlook.com.

Xinlei Wu received the B.S. degree in Mechanical Design & Manufacture and Automation at *China University of Petroleum (East China)* in 2015. He is currently working toward the Ph.D. degree in Mechanical Engineering under the supervision of Prof. Yonghong Liu. His present research interests mainly focus on non-traditional machining, intelligent manufacturing and machine learning. Tel: +86-18353244270; E-mail: wuxl@s.upc.edu.cn.

Qiang Sun, born in 1990, is currently a PhD candidate at College of Mechanical and Electronic Engineering, *China University of Petroleum (East China)*, His research interests include plasma drilling direction and plasma cutting technology. E-mail: sunqiang_upc@163.com.

Peng Liu received his Ph.D. degree in College of *Mechanical and Electronic Engineering from China University of Petroleum (East China)* in 2020. His recent research interests include reliability engineering, fault diagnosis, and Bayesian Networks methodology and application. E-mail: liupeng@s.upc.edu.cn.

Hang Dong received his Ph.D. degree in College of *Mechanical and Electronic Engineering from China University of Petroleum (East China)* in 2020. His recent research interests are non-traditional machining, advanced manufacturing technology. E-mail: donghang@xju.edu.cn.

Chi Ma, born in 1994, is currently a PhD candidate at College of Mechanical and Electronic Engineering, *China University of Petroleum (East China)*, China. He received his bachelor degree from *China University of Petroleum (East China)*, China, in 2017. His research interests include additive manufacturing and control. Tel: +86-15689138431; E-mail: b17040151@s.upc.edu.cn.

Dege Li, born in 1993, received bachelor's degree of mechanical engineering from *China University of Petroleum (East China)* in 2016, and now working towards his PhD at *China University of Petroleum (East China)*. His research interests involve the fabrication of microfluidic systems, ultra-fine droplet generation and manipulation, and satellite droplets mechanism. Tel: +86-13045043343; E-mail: lidege@s.upc.edu.cn.

Baoping Cai received B.S. degree in Mechanical Design, Manufacturing and Automation from China University of Petroleum in 2006. He received his Ph.D. degree in Mechanical and Electronic Engineering from *China University of Petroleum* in 2012. He is a lecturer in the same university from 2013 to 2014. Currently, he is a professor in *China University of Petroleum*. His research interests include reliability engineering, fault diagnosis, risk analysis, and Bayesian Networks methodology and application.

Competing Interests

The authors declare no competing financial interests.

Acknowledgements

Not applicable

Funding

Supported by National Natural Science Foundation of China

(Grant No. 51675535); the Major Research Project of Shandong Province (Grant No. 2019GGX104068); the Key Pre-Research Foundation of Military Equipment of China (Grant No. 6140923030702); the National Science and Technology Major Project (Grant No. 2017ZX05072) and the Science and Technology Support Plan for Youth Innovation of Universities in Shandong Province (Grant No.2019KJB016).

References

[1] R Li, Y Hou, B Liu, et al. Electrodeposition of homogenous Ni/SiO_2 nanocomposite coatings from deep eutectic solvent with in-situ synthesized SiO_2 nanoparticles. *Electrochimica Acta*, 2016, 222: 1272-1280.

[2] B Li, D Li, W Chen, et al. Effect of current density and deposition time on microstructure and corrosion resistance of Ni-W/TiN nanocomposite coating. *Ceramics International*, 2019, 45(4): 4870-4879.

[3] Y Tao, F Ma, M Teng, et al. Designed fabrication of super high hardness Ni-B-Sc nanocomposite coating for anti-wear application. *Applied Surface Science*, 2019, 492: 426-434.

[4] M Alizadeh, A Cheshmpish. Electrodeposition of Ni-Mo/Al_2O_3 nano-composite coatings at various deposition current densities. *Applied Surface Science*, 2019, 466: 433-440.

[5] S Banthia, S Sengupta, S Das, et al. Synthesis and characterization of novel Cu, Cu-SiC functionally graded coating by pulse reverse electrodeposition[J]. *Applied Surface Science*, 2019, 467-468: 567-579.

[6] C Wang, L Shen, M Qiu, et al. Characterizations of Ni-CeO_2 nanocomposite coating by interlaced jet electrodeposition. *Journal of Alloys and Compounds*, 2017, 727: 269-277.

[7] C Ma, W Yu, M Jiang, et al. Jet pulse electrodeposition and characterization of Ni–AlN nanocoatings in presence of ultrasound. *Ceramics International*, 2018, 44(5): 5163-5170.

[8] W Jiang, L Shen, M Qiu, et al. Preparation of Ni-SiC composite coatings by magnetic field-enhanced jet electrodeposition. *Journal of Alloys and Compounds*, 2018,762: 115-124.

[9] W Cui, K Wang, F Xia, et al. Simulation and characterization of Ni–doped SiC nanocoatings prepared by jet electrodeposition. *Ceramics International*, 2018, 44(5): 5500-5505.

[10] F F Xia, W C Jia, C Y Ma, et al. Synthesis and characterization of Ni-doped TiN thin films deposited by jet electrodeposition. *Applied Surface Science*, 2018, 434: 228-233.

[11] H Gao, W Zhen, J Ma, et al. High efficient solar hydrogen generation by modulation of Co-Ni sulfide (220) surface structure and adjusting adsorption hydrogen energy. *Applied Catalysis B: Environmental*, 2017, 206: 353-363.

[12] A Ponrouch, S Garbarino, E Bertin, et al. Highly Porous and Preferentially Oriented {100} Platinum Nanowires and Thin Films. *Advanced Functional Materials*, 2012, 22(19): 4172-4181.

[13] J Kim, K H Lee, S W Kim, et al. Potential-current co-adjusted pulse electrodeposition for highly (110)-oriented $Bi_2Te_{3-x}Se_x$ films. *Journal of Alloys and Compounds*, 2019, 787: 767-771.

[14] J A Calderón, J E Henao, M A Gómez. Erosion–corrosion resistance of Ni composite coatings with embedded SiC nanoparticles. *Electrochimica Acta*, 2014, 124: 190-198.

[15] Y Zhao, L Wang, Y Sun, et al. Influences of Al and Ti particles on microstructure, internal stress and property of Ni composite coatings. *Journal of Alloys and Compounds*, 2019, 793: 314-325.

[16] M Alizadeh, H Safaei. Characterization of Ni-Cu matrix, Al_2O_3 reinforced nano-composite coatings prepared by electrodeposition. *Applied Surface Science*, 2018, 456: 195-203.

[17] J Deng, J Zhang, Y Tu, et al. Effect of BEO in the electrodeposition process of Ni/diamond composite coatings for preparation of ultra-thin dicing blades: Experiments and theoretical calculations. *Ceramics International,* 2018, 44(14): 16828-16836.

[18] R Ji, K Han, H Jin , et al. Preparation of Ni-SiC nano-composite coating by rotating magnetic field-assisted electrodeposition. *Journal of Manufacturing Processes*, 2020, 57:787-797.

[19] N Guglielmi. Kinetics of the Deposition of Inert Particles from Electrolytic Baths. *Journal of the Electrochemical Society*, 1972, 119(8): 1009.

[20] J P Celis, J R Roos, C Buelens. A Mathematical Model for the Electrolytic Codeposition of Particles with a Metallic Matrix. *Journal of the Electrochemical Society*, 2019, 134(6): 1402-1408.

[21] S Xie, M Dai, S Lin, et al. Effect of bias voltage on the oxidation resistance of NiCoCrAlYTa coatings prepared by arc ion plating. *Corrosion Science*, 2019, 147: 330-341.

[22] X Chen, X Qin, Z Zhu, et al. Microstructural evolution and wear properties of the continual local induction cladding NiCrBSi coatings. *Journal of Materials Processing Technology*, 2018, 262: 257-268.

[23] Y E Sknar, O O Savchuk, I V Sknar. Characteristics of electrodeposition of Ni and Ni-P alloys from methanesulfonate electrolytes. *Applied Surface Science*, 2017, 423: 340-348.

[24] S Kumaraguru, G G Kumar, S Shanmugan, et al. Enhanced texture and microhardness of the nickel surface using Bi_2O_3 particles via electrodeposition technique for engineering application. *Journal of Alloys and Compounds*, 2018, 753: 740-747.

[25] B Li, W Zhang, W Zhang, et al. Preparation of Ni-W/SiC nanocomposite coatings by electrochemical deposition. *Journal of Alloys and Compounds,* 2017, 702: 38-50.

[26] Y Lv, Y Ding, H Cui, et al. Investigation of microscopic residual stress and its effects on stress corrosion behavior of NiAl bronze alloy using in situ neutron diffraction/EBSD/tensile corrosion experiment. *Materials Characterization*, 2020, 164: 110351.

[27] F Zhang, R Ji, Y Liu, et al. Defect-rich Engineering and F Dopant Co-modulated NiO Hollow Dendritic Skeleton as A Self-Supported Electrode for High-Current Density Hydrogen Evolution Reaction. *Chemical Engineering Journal*, 2020:126037.

[28] F Zhang, R Ji, Y Liu, et al. A novel nickel-based honeycomb electrode with microtapered holes and abundant multivacancies for highly efficient overall water splitting. *Applied Catalysis B: Environmental*, 2020, 276:119141.

[29] R Ji, F Zhang, Y Liu, et al. Simple synthesis of a vacancy-rich NiO 2D/3D dendritic self-supported electrode for efficient overall water splitting. *Nanoscale*, 2019, 11.

[30] Q Liu, X Cao, A Du, et al. Investigation on adhesion strength and corrosion resistance of Ti-Zr aminotrimethylene phosphonic acid composite conversion coating on 7A52 aluminum alloy. *Applied Surface Science,* 2018, 458: 350-359.

[31] H J M Soares, O S Campos, D F Dias, et al. Chemical, morphological and corrosion characterisations of electrodeposited Ni-Fe-P coatings. *Electrochimica Acta,* 2018, 284: 18-23.

[32] Z Chai, C Jiang. Corrosion behavior and product film formation of Ni-Co-Cu nanocrystalline coatings in neutral salt environments. *Electrochimica Acta,* 2019, 298: 616-629.

[33] Z Mei, S Bhattacharya, A M Yacout. Adhesion of ZrN and Al_2O_3

coatings on U metal from first-principles. *Applied Surface Science,* 2019, 473: 121-126.

[34] D Yin, X Peng, Y Qin, et al. Quantifying adhesion energy of mechanical coatings at atomistic scale. *Applied Surface Science*, 2011, 258(4): 1451-1455.

Figures

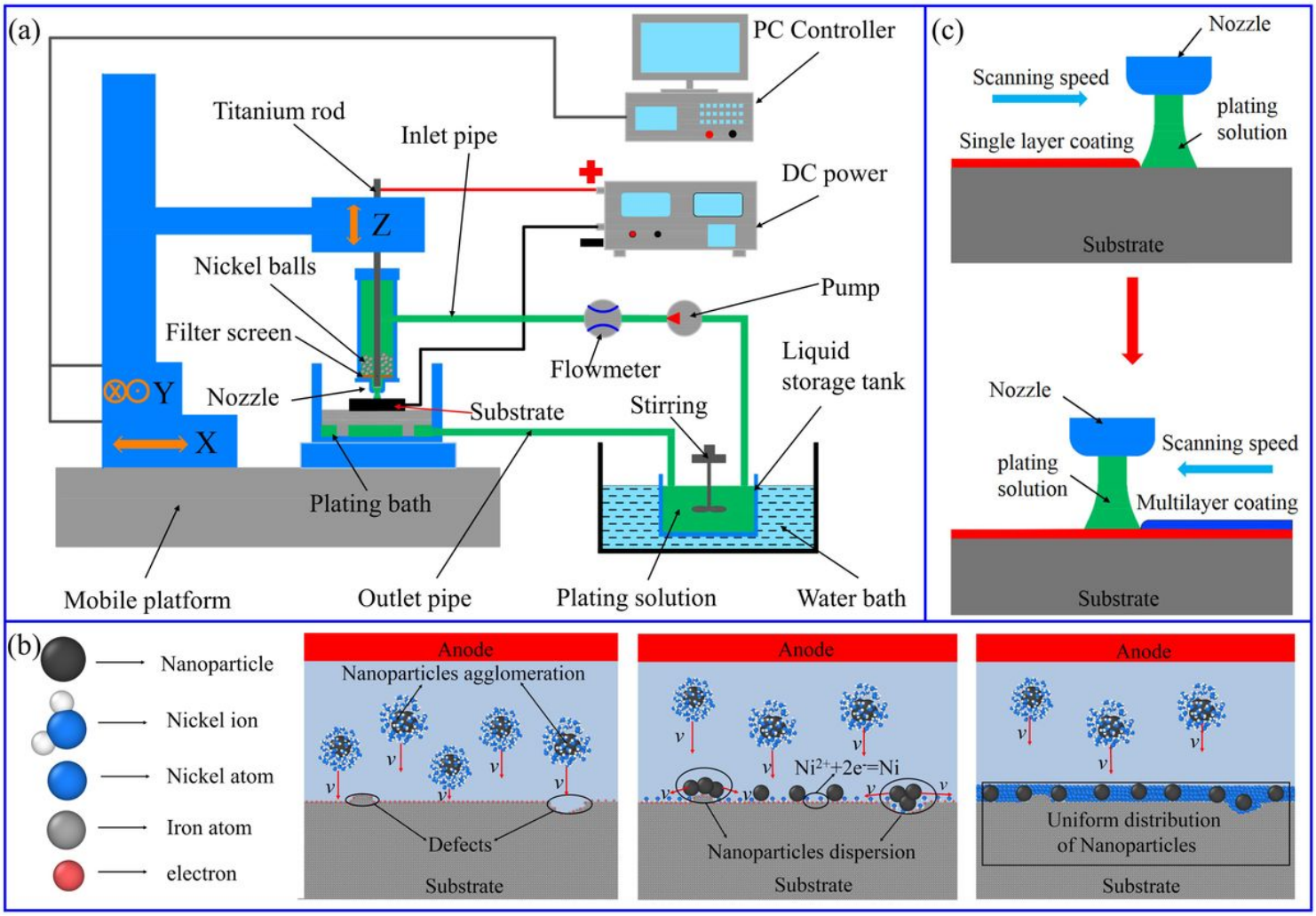

Figure 1

Schematic diagram of (a) experimental device for JED, (b) preparation principle of nanoparticles reinforced nickel-based composite coatings, (c) production process of nanoparticles reinforced nickel-based composite coatings.

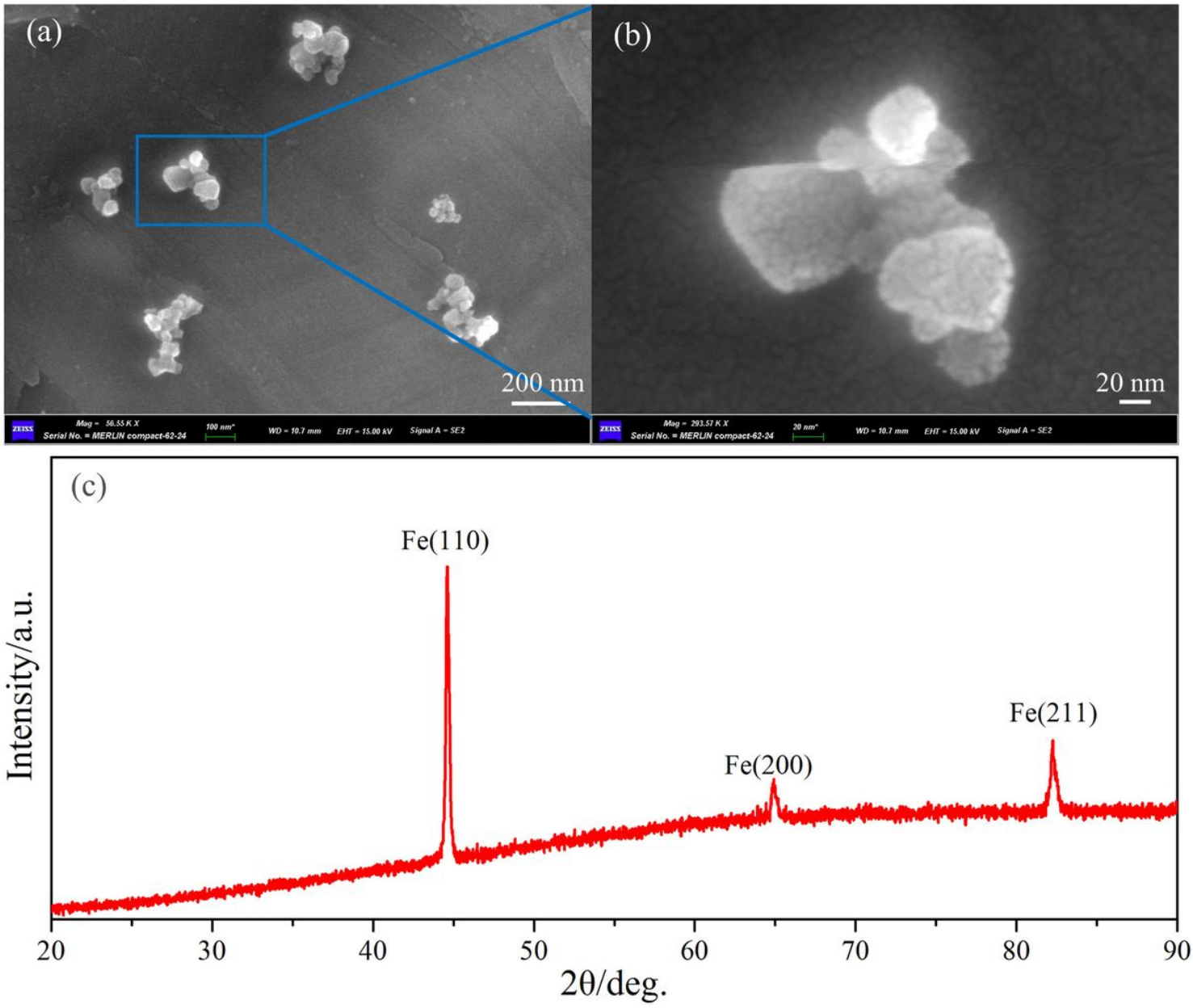

Figure 2

The morphology and composition of SiC nanoparticles: (a) SEM image, (b) enlarged image, (c) XRD pattern of substrate.

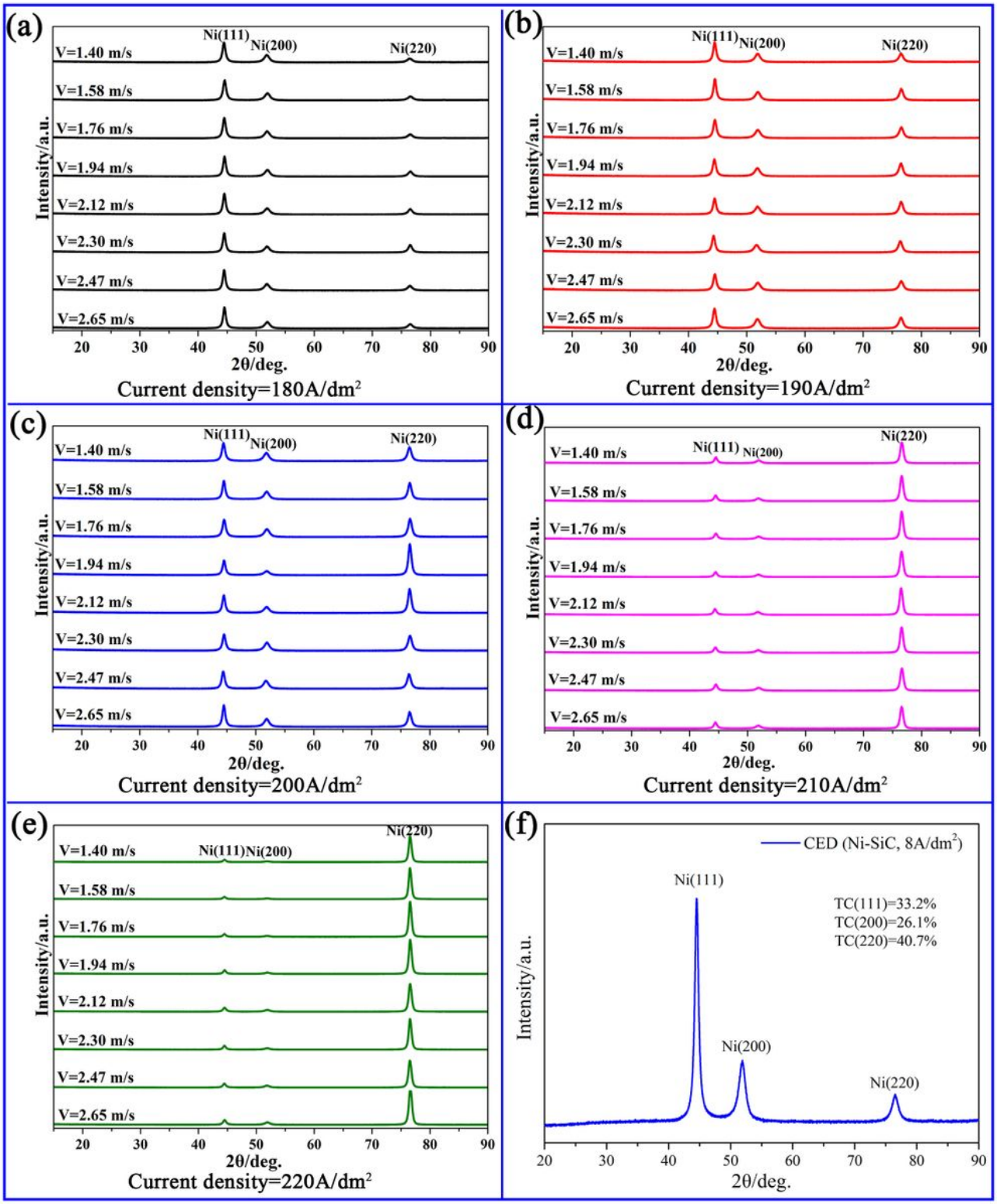

Figure 3

(a-e) XRD patterns of Ni-SiC composite coatings prepared by JED under different deposition parameters, (f) XRD pattern of Ni-SiC composite coating prepared by CED.

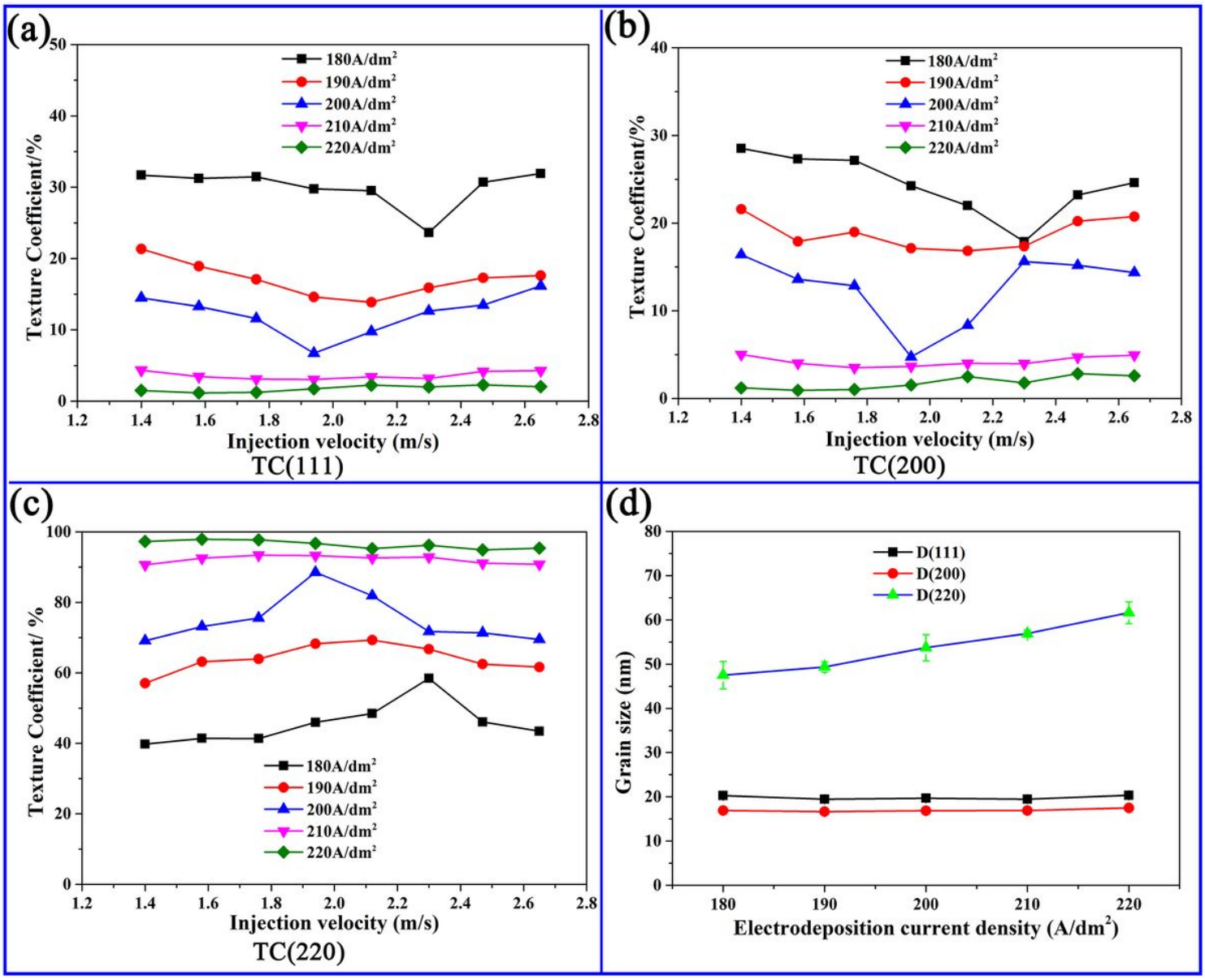

Figure 4

(a-c) The texture coefficients of Ni-SiC composite coatings prepared by JED under different deposition parameters: (a) TC(111), (b) TC(200), (c) TC(220). (d) The grain size statistic of Ni-SiC composite coatings prepared by JED under different deposition parameters.

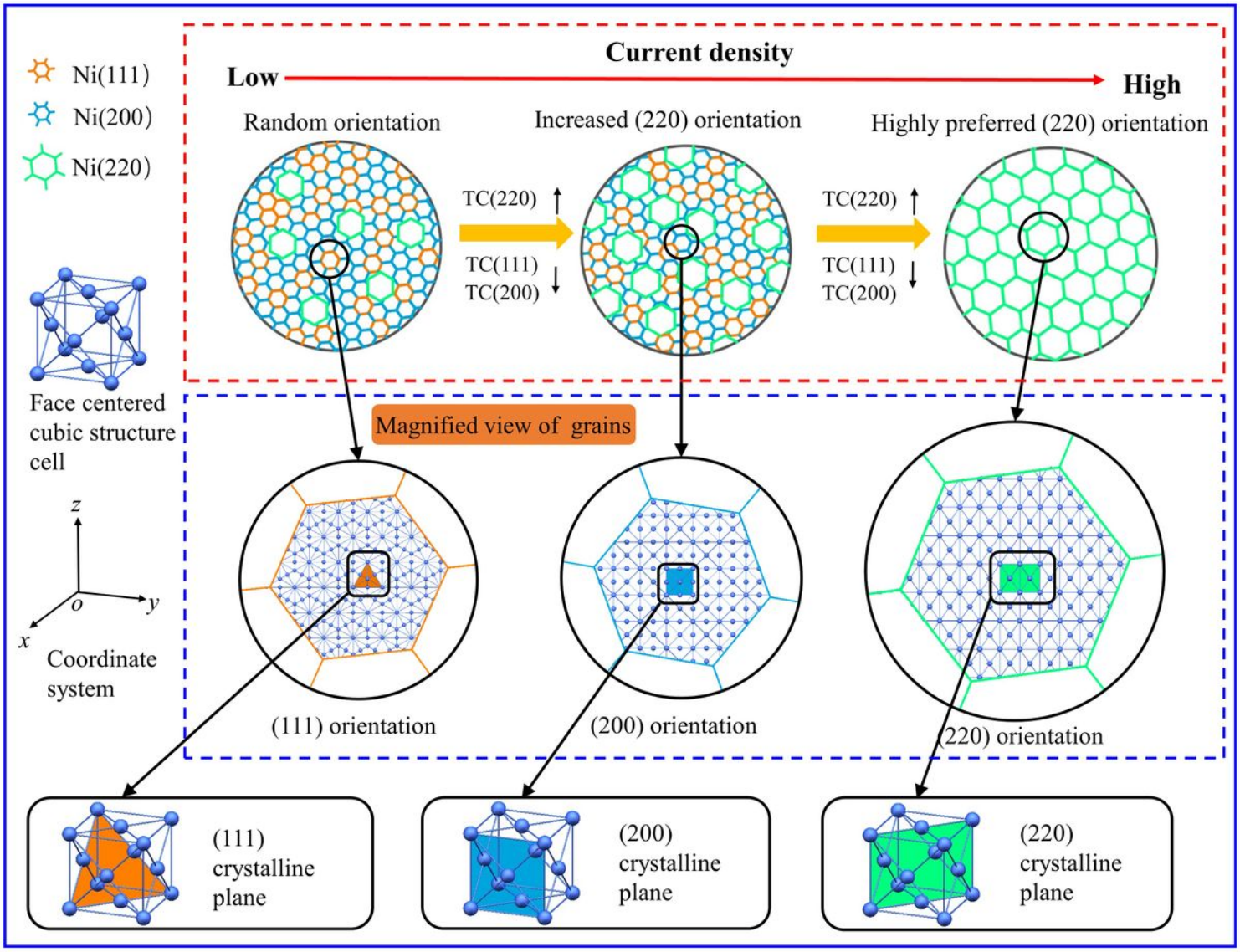

Figure 5

Schematic diagram of the evolution of grain orientation in the process of preparing nanoparticles reinforced nickel-based composite coatings by JED.

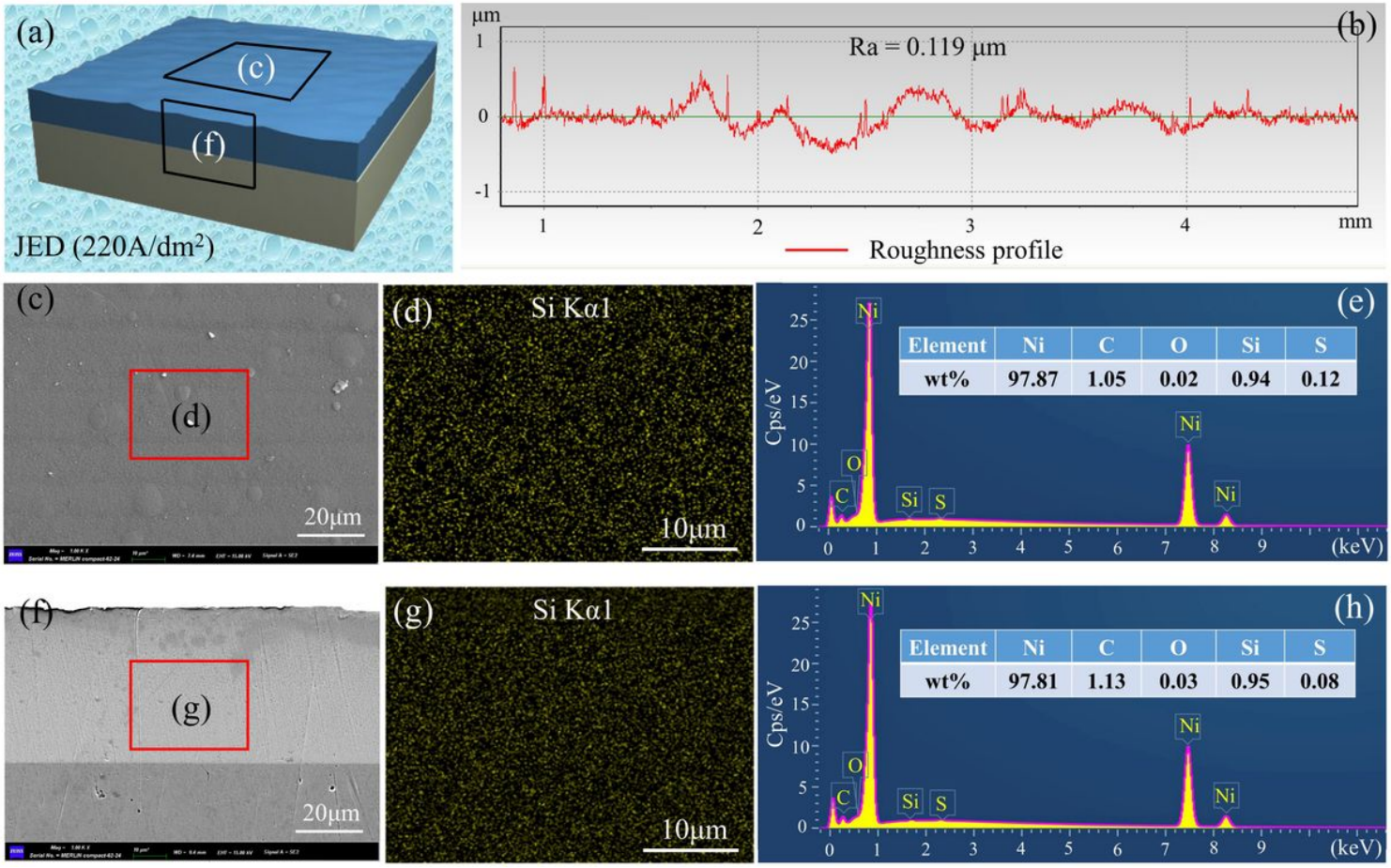

Figure 6

The morphology of the Ni-SiC composite coating with highly preferred (220) orientation prepared by JED: (a) schematic diagram of detection area, (b) roughness profile of the coating surface, (c) microstructure of the coating surface, (d) distribution of SiC nanoparticles on the coating surface, (e) EDS map of the coating surface, (f) microstructure of the coating section, (g) distribution of SiC nanoparticles on the coating section, (h) EDS map of the coating section.

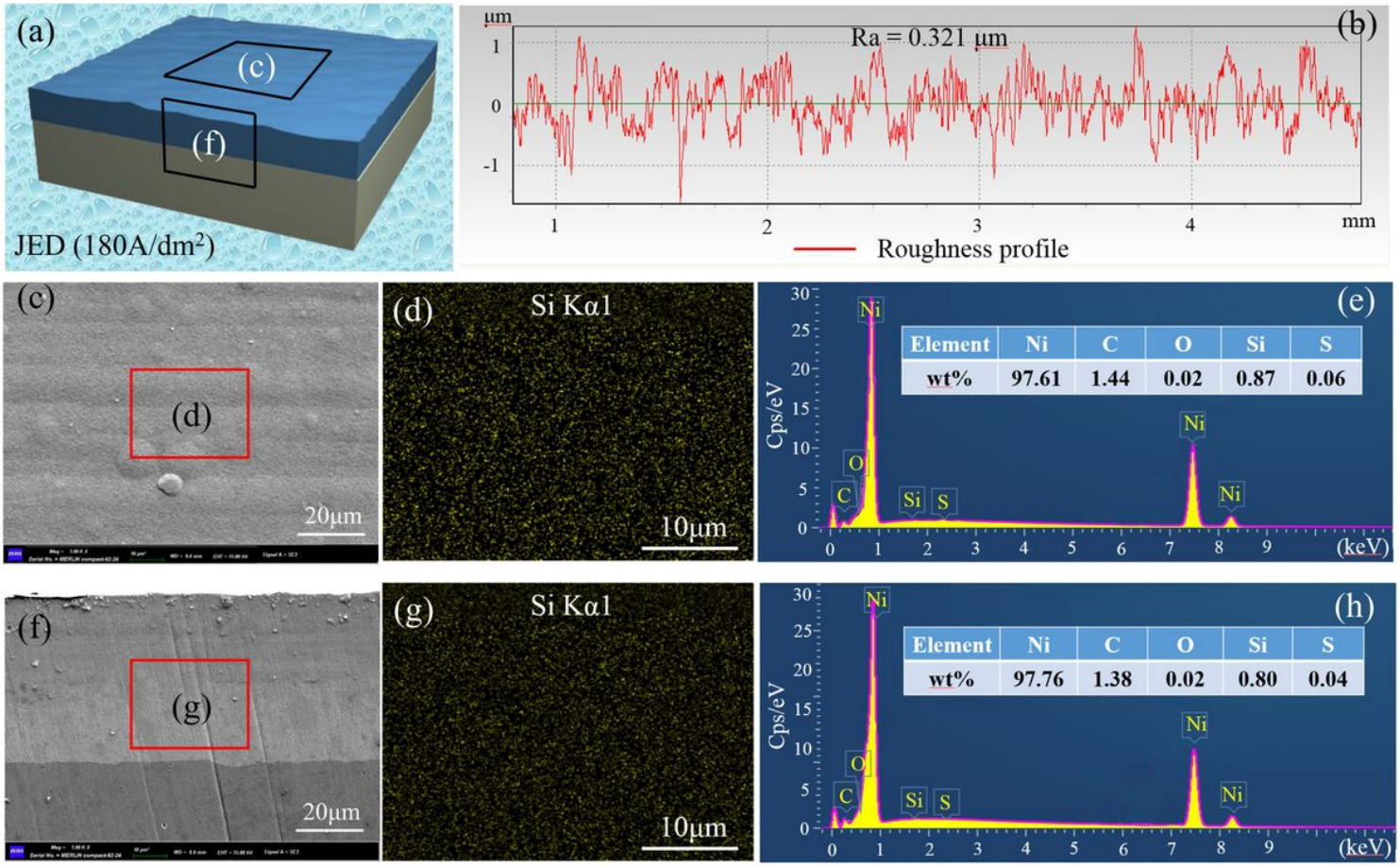

Figure 7

The morphology of the Ni-SiC composite coating without highly preferred (220) orientation prepared by JED: (a) schematic diagram of detection area, (b) roughness profile of the coating surface, (c) microstructure of the coating surface, (d) distribution of SiC nanoparticles on the coating surface, (e) EDS map of the coating surface, (f) microstructure of the coating section, (g) distribution of SiC nanoparticles on the coating section, (h) EDS map of the coating section.

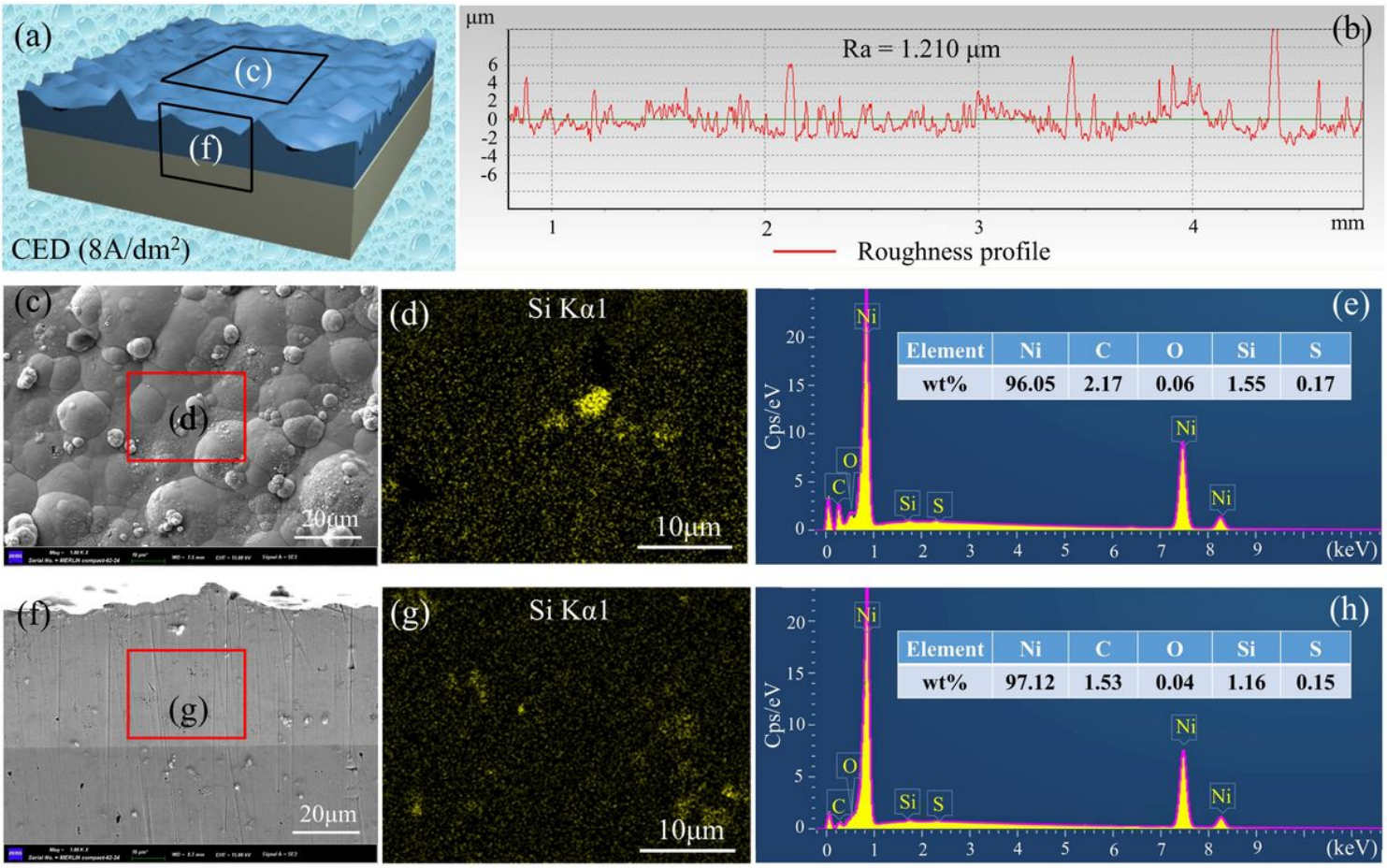

Figure 8

The morphology of the Ni-SiC composite prepared by CED: (a) schematic diagram of detection area, (b) roughness profile of the coating surface, (c) microstructure of the coating surface, (d) distribution of SiC nanoparticles on the coating surface, (e) EDS map of the coating surface, (f) microstructure of the coating section, (g) distribution of SiC nanoparticles on the coating section, (h) EDS map of the coating section.

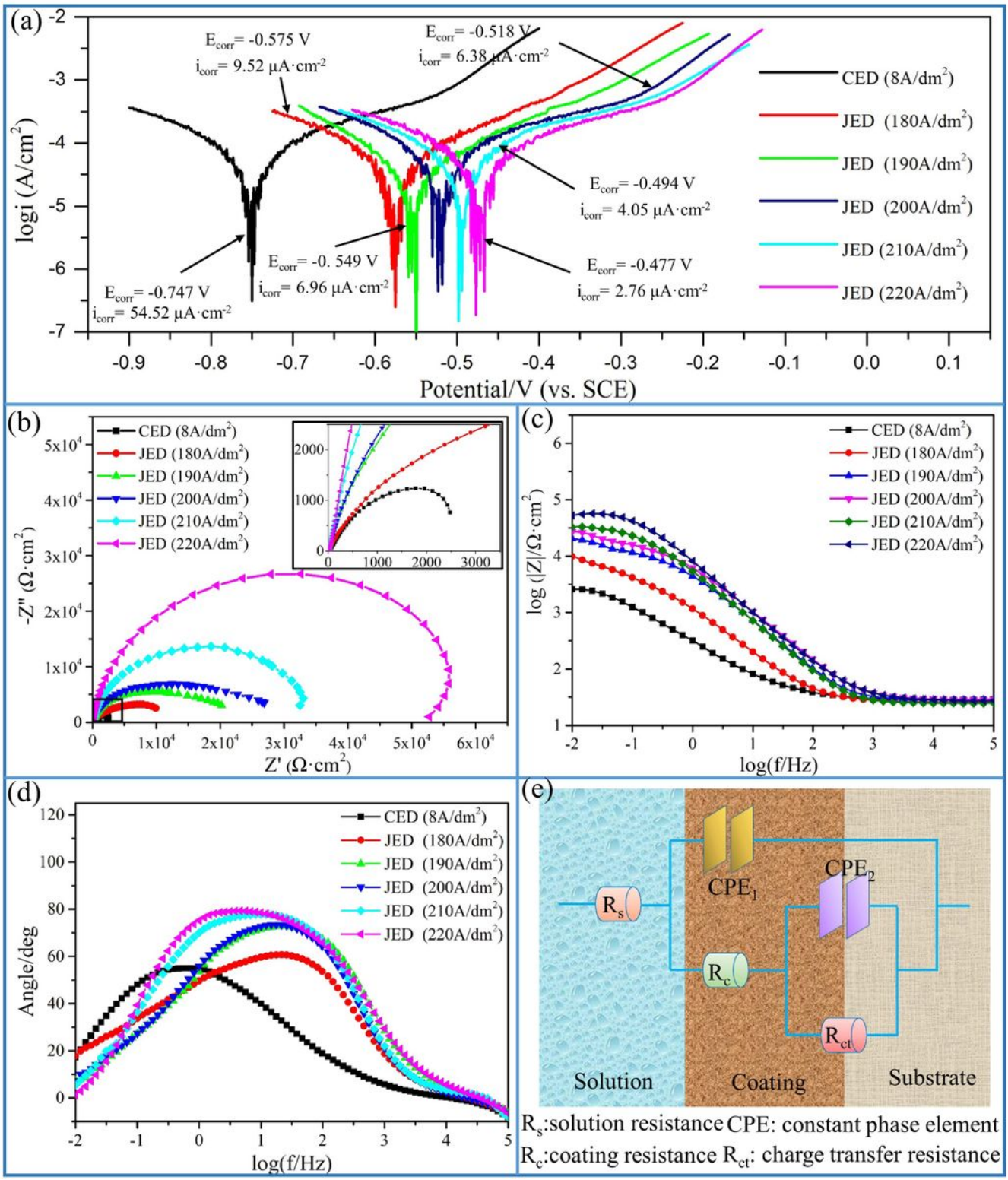

Figure 9

Electrochemical test results of Ni-SiC composite coatings: (a) dynamic polarization curves, (b) Nyquist plots, (c) Bode plots of log(f) vs. log(|Z|), (d) Bode plots of log(f) vs. Angle, (e) schematic diagram of the EEC.

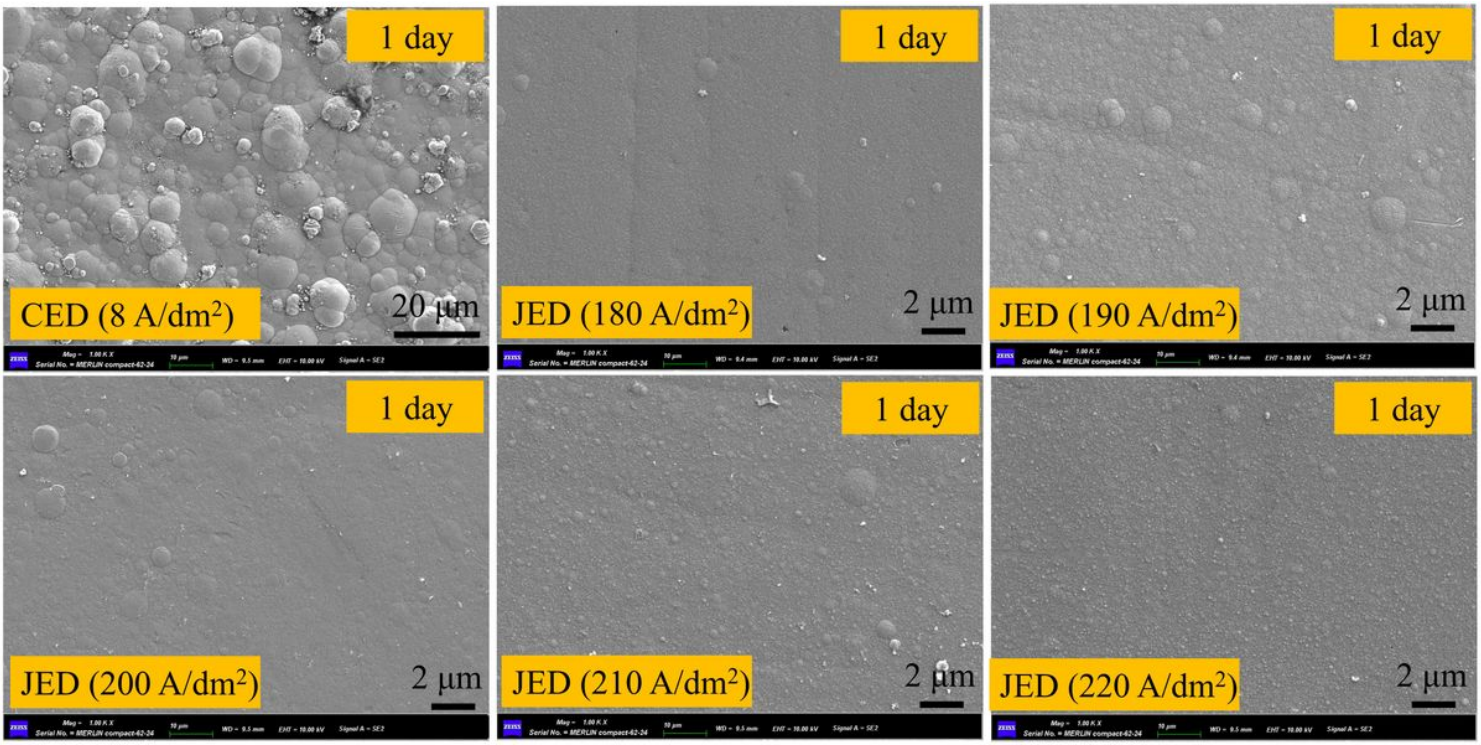

Figure 10

The surface morphologies of different Ni-SiC composite coatings after 1 day of immersion corrosion in 3.5 wt% NaCl solution

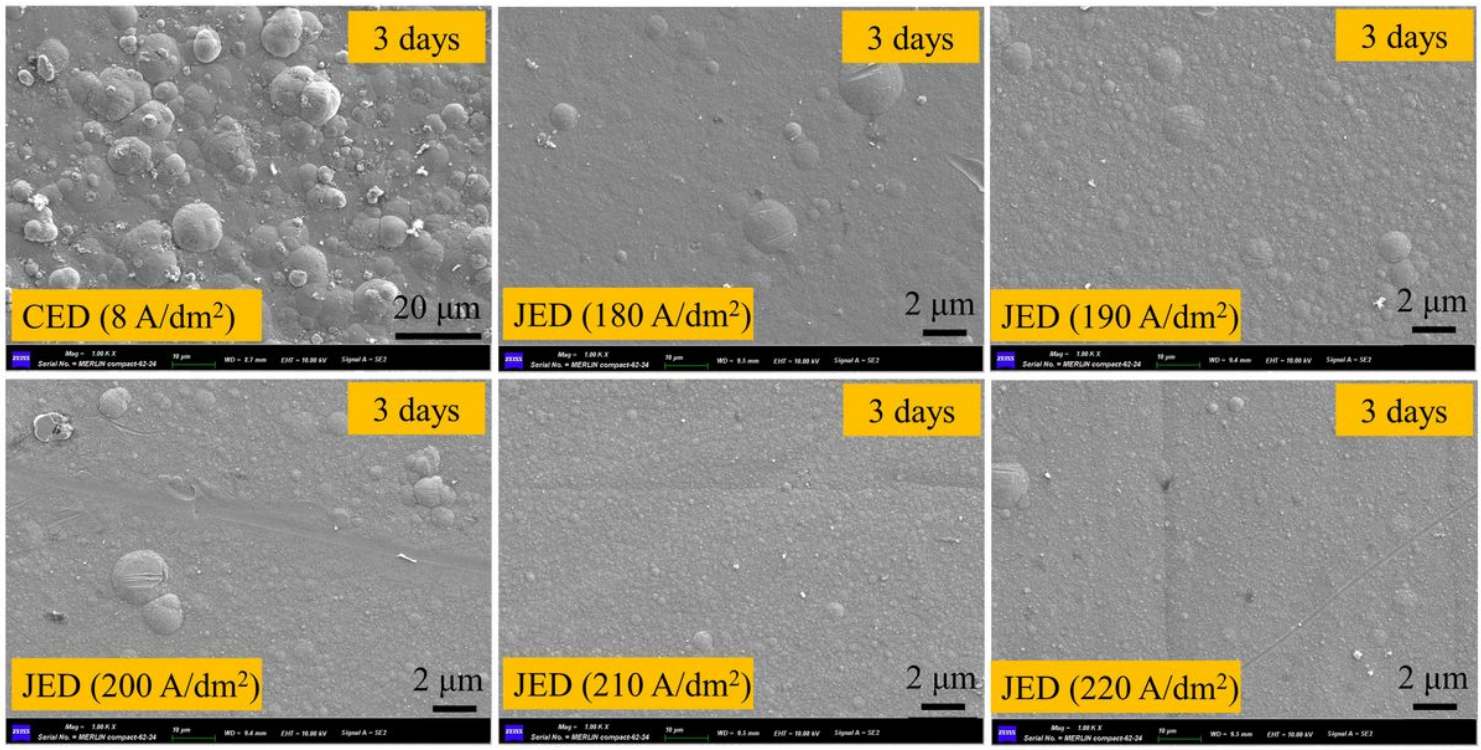

Figure 11

The surface morphologies of different Ni-SiC composite coatings after 3 days of immersion corrosion in 3.5 wt% NaCl solution.

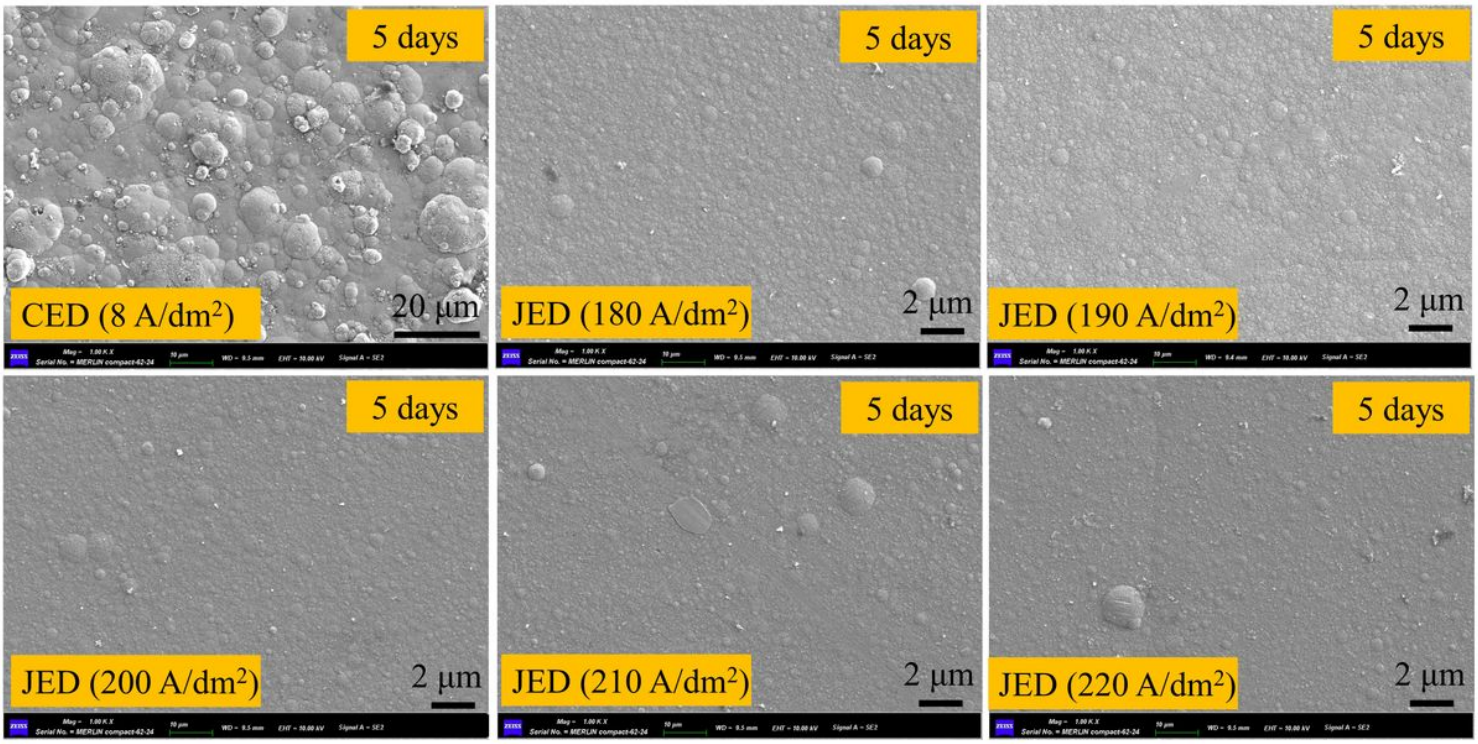

Figure 12

The surface morphologies of different Ni-SiC composite coatings after 5 days of immersion corrosion in 3.5 wt% NaCl solution.

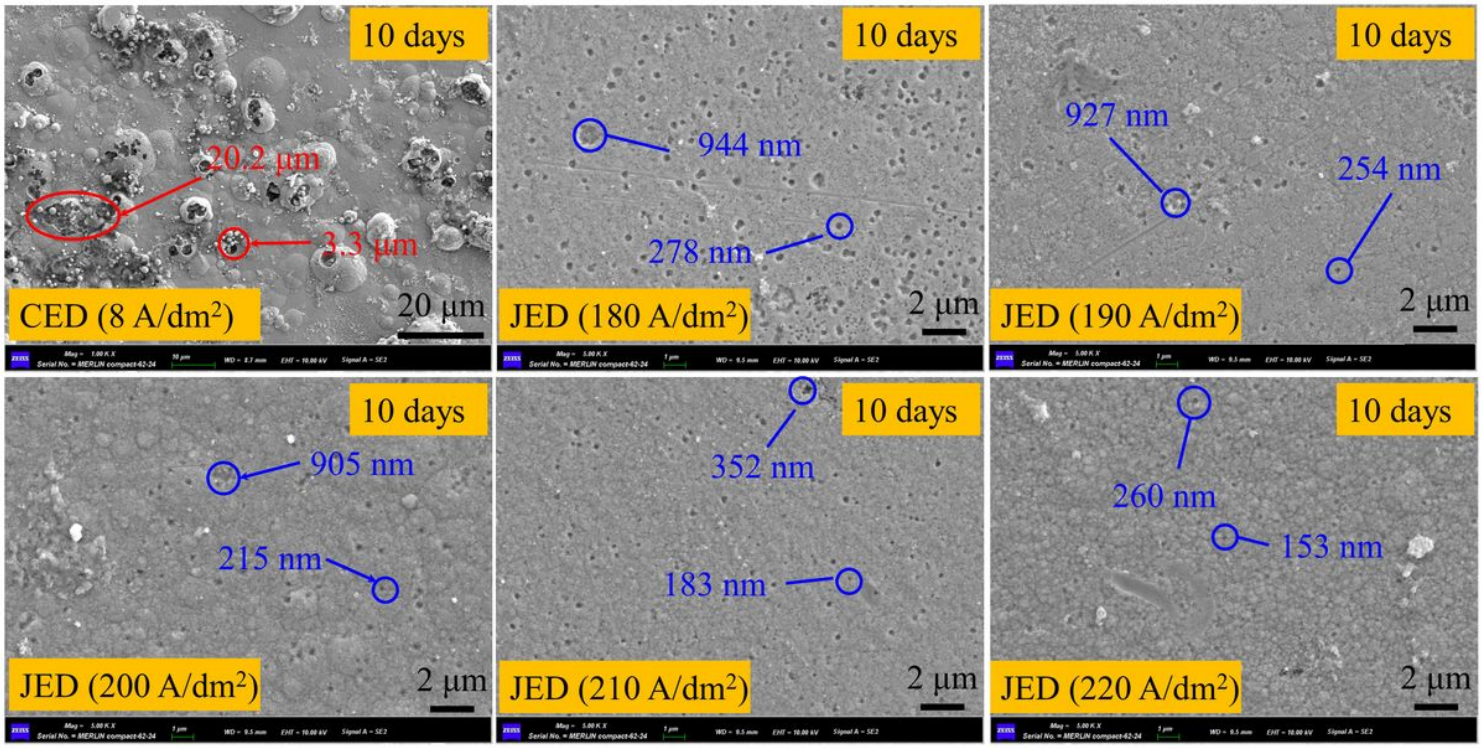

Figure 13

The surface morphologies of different Ni-SiC composite coatings after 10 days of immersion corrosion in 3.5 wt% NaCl solution.

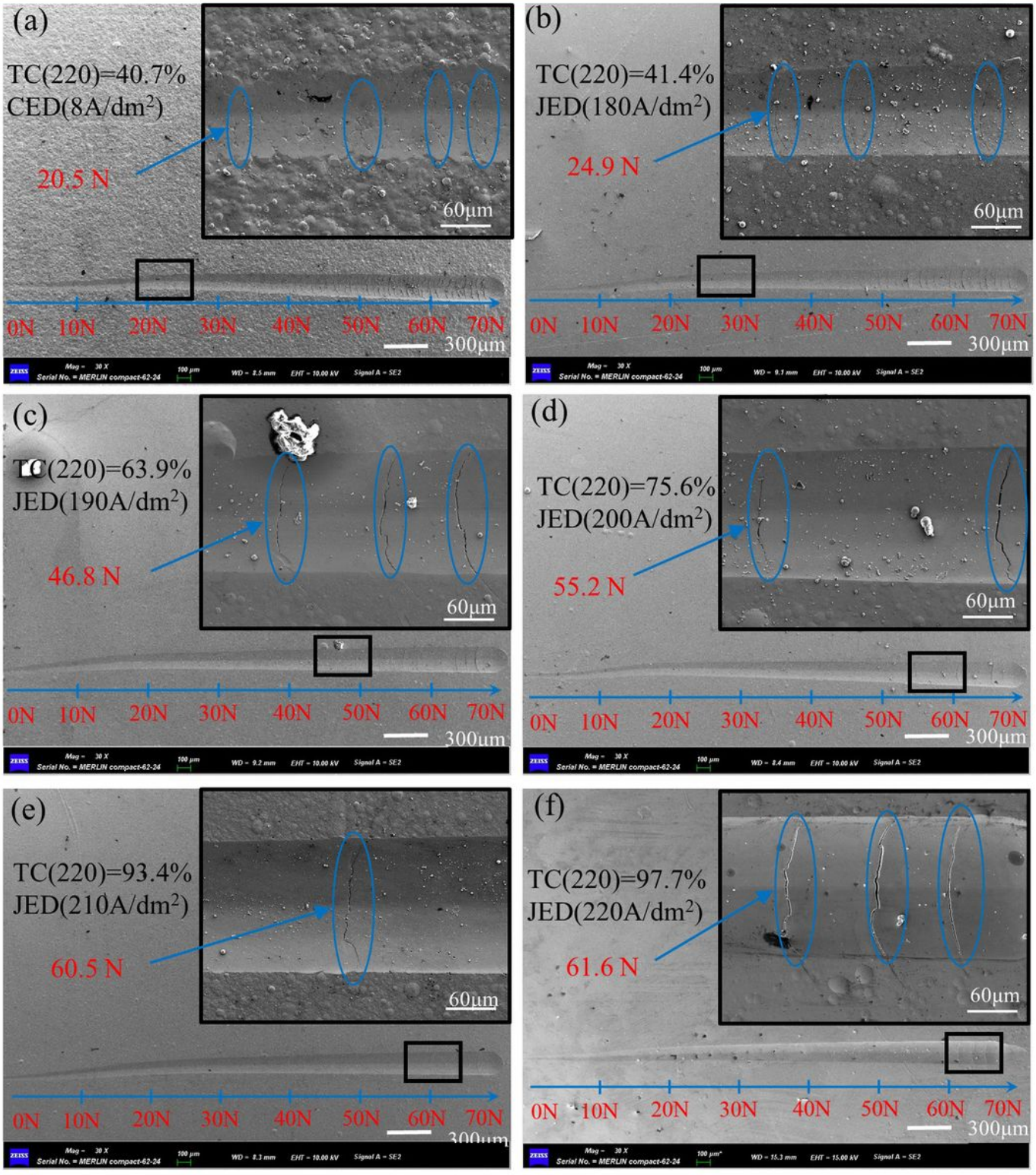

Figure 14

(a-f) Scratch morphology of different Ni-SiC composite coatings: (a) CED (8 A/dm2), (b) JED (180 A/dm2), (c) JED (190 A/dm2), (d) JED (200 A/dm2), (e) JED (210 A/dm2), (f) JED (220 A/dm2).

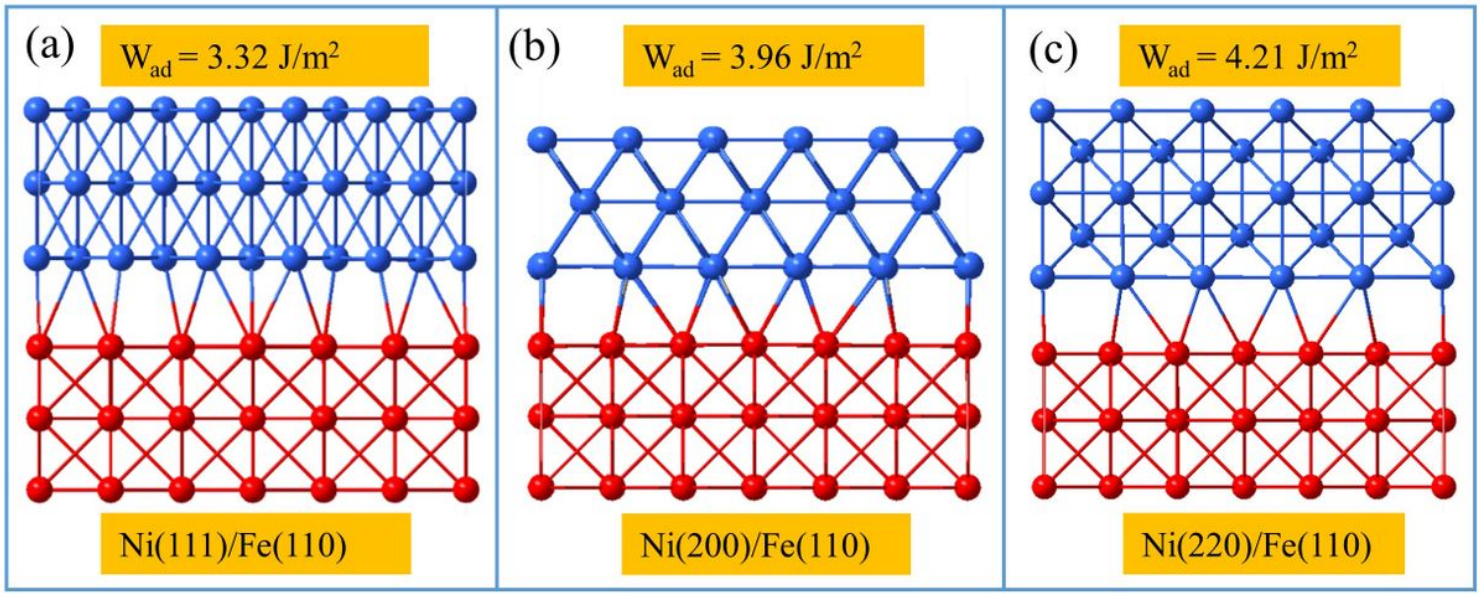

Figure 15

DFT optimized structures of (a) Ni(111)/Fe(110), (b) Ni(200)/Fe(110) and (c) Ni(220)/Fe(110) interfaces.

Supplementary Files

This is a list of supplementary files associated with this preprint. Click to download.

- SupportingInformation.docx